Nucleic Acids Research, 2024, **52**, 8466–8482
https://doi.org/10.1093/nar/gkae387
Advance access publication date: 20 May 2024
RNA and RNA-protein complexes

Arabidopsis AGO1 N-terminal extension acts as an essential hub for PRMT5 interaction and post-translational modifications

Andrea Martín-Merchán [1,†], Antonela Lavatelli [1,†], Camila Engler [1], Víctor M. González-Miguel [1], Belén Moro [1], Germán L. Rosano [2] and Nicolas G. Bologna [1,*]

[1]Centre for Research in Agricultural Genomics (CRAG), CSIC-IRTA-UAB-UB, Bellaterra, Barcelona 08193, Spain
[2]Institute of Molecular and Cellular Biology of Rosario, Rosario, Argentina

[*]To whom correspondence should be addressed. Tel: +34 935636600 (Ext. 3211); Email: nicolas.bologna@cragenomica.es
[†]The first two authors should be regarded as Joint First Authors.

Abstract

Plant ARGONAUTE (AGO) proteins play pivotal roles regulating gene expression through small RNA (sRNA) -guided mechanisms. Among the 10 AGO proteins in *Arabidopsis thaliana*, AGO1 stands out as the main effector of post-transcriptional gene silencing. Intriguingly, a specific region of AGO1, its N-terminal extension (NTE), has garnered attention in recent studies due to its involvement in diverse regulatory functions, including subcellular localization, sRNA loading and interactions with regulatory factors. In the field of post-translational modifications (PTMs), little is known about arginine methylation in Arabidopsis AGOs. In this study, we show that NTE of AGO1 (NTE^{AGO1}) undergoes symmetric arginine dimethylation at specific residues. Moreover, NTE^{AGO1} interacts with the methyltransferase PRMT5, which catalyzes its methylation. Notably, we observed that the lack of symmetric dimethylarginine has no discernible impact on AGO1's subcellular localization or miRNA loading capabilities. However, the absence of PRMT5 significantly alters the loading of a subgroup of sRNAs into AGO1 and reshapes the NTE^{AGO1} interactome. Importantly, our research shows that symmetric arginine dimethylation of NTEs is a common process among Arabidopsis AGOs, with AGO1, AGO2, AGO3 and AGO5 undergoing this PTM. Overall, this work deepens our understanding of PTMs in the intricate landscape of RNA-associated gene regulation.

Graphical abstract

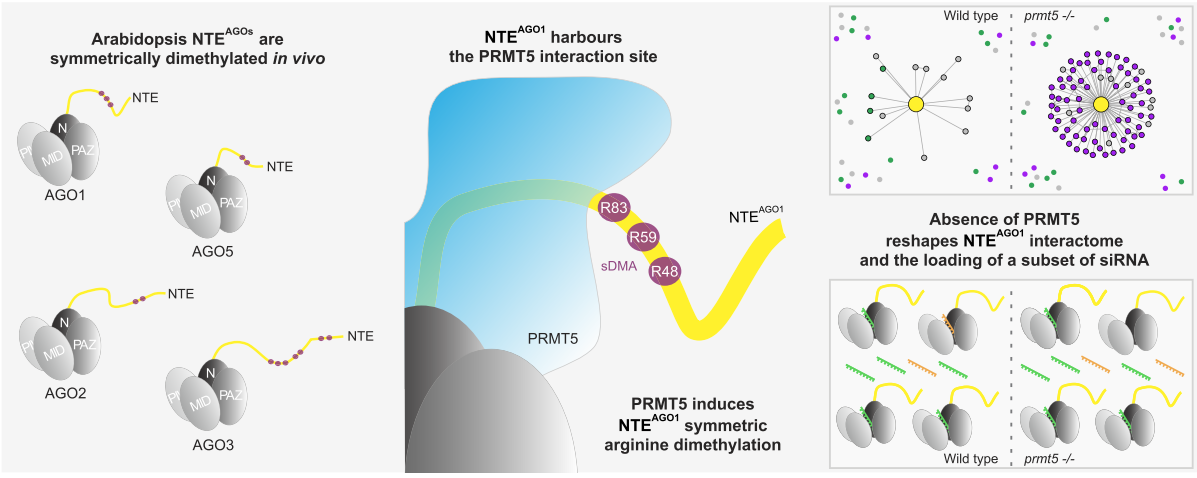

Introduction

RNA silencing regulates gene expression via 19–32 nucleotide (nt) small RNAs (sRNAs). In plants, sRNAs (20–24nt) play key roles in development, as well as biotic and abiotic stress responses. At the molecular level, sRNAs control gene expression by regulating chromatin modifications, transcript abundance, and protein translation through diverse mechanisms. Plant sRNAs can be divided into two main classes: microRNAs (miRNAs, 20–22nt) and small interfering RNAs (siRNAs, 21–24nt). Although each sRNA pathway possesses specific characteristics, the fundamental mechanism falls into four common steps: (i) induction by double-stranded RNA (dsRNA); (ii) dsRNA processing by DICER-LIKE proteins into sRNA duplexes; (iii) methylation of sRNA by HUA

Received: November 2, 2023. **Revised:** April 10, 2024. **Editorial Decision:** April 25, 2024. **Accepted:** April 30, 2024

ENHANCER1; and (iv) incorporation of sRNA into RNA-induced silencing complexes (RISCs) (1,2).

ARGONAUTE (AGO) proteins constitute the main component of RISCs, recruiting miRNAs/siRNAs to pair with the target RNAs, thereby regulating them at transcriptional or post-transcriptional levels (3,4). Eukaryotic AGO proteins can be phylogenetically divided into three different subfamilies: the AGO subfamily, the PIWI subfamily (present only in metazoans), and the worm-specific AGO (WAGO) subfamily. AGO proteins are composed of several highly conserved domains: N, PAZ, MID and PIWI, interconnected by two linker (L1 and L2) domains (5,6). Each AGO domain serves specific functions relevant to the diverse physiological roles of AGO proteins. For example, while the N domain was described as serving as a wedge to split duplexes during the RISC assembly (7), the PAZ and MID domains recognize the 3 and 5 ends of the sRNA, respectively (8,9), and the PIWI domain enables the RNA cleavage (10). In addition to the conserved domains, all AGO proteins feature an unstructured (N)amino-terminal extension (NTE) located upstream of the N domain. NTEs are highly variable and typically rich in amino acid residues that enhance flexibility, constituting a disordered and presumably solvent-exposed segment (11). The Arabidopsis genome encodes ten AGO proteins distributed among three different clades: AGO1/5/10 (clade I), AGO2/3/7 (clade II), and AGO4/6/8/9 (clade III) (12). Clade I AGO proteins primarily execute post-transcriptional gene silencing (PTGS) and predominantly localize to the cytoplasm. In contrast, clade III AGOs participate in transcriptional gene silencing (TGS) and exhibit mainly nuclear subcellular localization. Clade II AGOs are involved in diverse functions (including secondary siRNA biogenesis, DNA repair and antiviral defense) and display dual nuclear-cytoplasmic subcellular localizations (11).

Plants´ NTEs have received little attention compared to the N, PAZ, MID and PIWI domains. Alignments of the ten AGO proteins from Arabidopsis reveal that NTEs vary in length and amino acid composition compared to the highly conserved amino acid sequences encompassing the globular domains (11). Recently, it was shown that NTE is indispensable for Arabidopsis AGO1 functions. AGO1´s NTE (NTE^{AGO1}) is essential for endoplasmic reticulum membrane association (13), subcellular shuttling of AGO1 (14), sRNA loading (15), and acts as a region of interaction for regulatory factors (16). These findings suggest that NTE^{AGO1} could potentially serve as a platform for controlling the functionality of this protein through a range of intricate mechanisms. AGO1 is the main effector of miRNA-mediated PTGS. It also mediates trans-acting siRNA (tasiRNA) biogenesis and activity, DNA repair processes, and plays an important role in antiviral silencing upon loading virus-derived siRNAs (11). AGO1 possesses a complex homeostasis network regulating protein levels under non-stress and stress conditions, at both messenger RNA (mRNA) and protein levels. At mRNA levels, AGO1 is negatively regulated by miR168, which interacts with a target site within AGO1's mRNA (17). At protein levels, AGO1 undergoes different post-translational modifications (PTMs). Ubiquitylation, a pivotal PTM, is crucial in AGO1 regulation with a prominent role during viral infections. In this process, a Poleovirus-encoded F-box protein, P0, ubiquitynates AGO1 by targeting the L2 linker. The P0-induced AGO1 degradation operates via the autophagy pathway, distinguishing it from the proteasome-mediated degradation (18,19). Phosphorylation has also been reported to occur in Arabidopsis AGO1, however, there is no conclusive evidence of the impact of this phosphorylation event on AGO1 function (20).

Arginine methylation is one of the most common PTM observed in nuclear and cytoplasmic proteins. Proteins subjected to arginine methylation participate in a wide range of cellular processes, from transcriptional regulation and signal transduction to RNA metabolism and DNA damage repair (21). At the molecular level, this modification entails the alteration of arginine residues' physicochemical properties, leading to changes in the structural conformation of the target proteins (22). Arginine methylation comprises three distinctive forms: (i) monomethylarginine (MMA), which involves the attachment of a single methyl group to one of arginine's terminal nitrogen atoms; (ii) asymmetric dimethylarginine (aDMA), which entails the addition of two methyl groups to the same arginine's terminal nitrogen; and (iii) symmetric dimethylarginine (sDMA), which is characterized by the placement of one methyl group on each of arginine's two terminal nitrogens. The enzymes that catalyze arginine methylation belong to a protein family named Protein Arginine Methyltransferases (PRMTs). PRMTs can be categorized into three distinct types: while all PRMT variants perform MMA formation, aDMA is produced by type I PRMTs, and sDMA by type II PRMTs. Type III PRMTs exclusively catalyze MMA formation (23). The Arabidopsis genome encodes nine PRMTs: seven type I (PRMT1a, PRMT1b, PRMT3, PRMT4a, PRMT4b, PRMT6 and PRMT10), one type II (PRMT5), and one type III (PRMT7) (24). PRMT-guided methylation predominantly occurs within the intrinsically disordered regions of proteins, frequently within glycine-arginine-rich (GAR) protein domains. These GAR domains include mainly well-known repeats such as RGG, RG and RXR (25). Several domains have been identified for recognizing methylarginine residues in proteins, including the Tudor domain found in proteins such as SMN (Survival of Motor Neuron), SPF30 (Splicing factor 30), and TDRD1/2/3/6/9/11 (Tudor domain-containing proteins) (26). In Arabidopsis, there are two Tudor-like proteins (TSN), TSN1 and TSN2, that contain four staphylococcal/micrococcal-like nuclease domains and a Tudor domain, and share homology with the human Tudor protein SND1 (27).

In recent years, the biological significance of symmetric arginine dimethylation in the NTE of AGO proteins has significantly increased, as it has been documented to occur in the NTEs of various PIWI proteins of worms, flies, mouse and humans (28–31). This process has been observed to influence both protein stability and functionality of these proteins. For example, in flies, symmetric arginine dimethylation of Ago3 and Aub by PRMT5 is vital for preserving protein stability (29), while in worms, the symmetric arginine dimethylation of the CSR-1a NTE provokes a selective binding of specific sRNAs implicated in spermatogenesis (31). Similarly, symmetric arginine dimethylation of the NTE of human PIWIL1 facilitates the interaction with Tudor proteins, thus ensuring Piwi-interacting RNA (piRNA) maturation (30). In plants, only Arabidopsis AGO2 has been reported to be methylated. Recently, it has been shown that symmetric arginine dimethylation promotes *At*-AGO2-TSN2 interaction and protein degradation (32). However, no studies have been performed on the main AGO effector for PTGS (AGO1) or TGS (AGO4) in any plant species.

In this study, we present compelling evidence that supports the occurrence of site-specific sDMA modification within

the NTE^{AGO1}. Additionally, we found that NTE^{AGO1} interacts with the methyltransferase PRMT5, which catalyzes its methylation. We observed that the lack of sDMAs has no discernible impact on AGO1's subcellular localization or miRNA loading capabilities. However, the absence of PRMT5 significantly alters the loading of a subgroup of siRNAs into AGO1 and reshapes the NTE^{AGO1} interactome. Importantly, our research extends beyond AGO1, illustrating that symmetric arginine dimethylation of NTEs is a common process across Arabidopsis AGOs, taking place in AGO1, AGO2, AGO3 and AGO5, deepening our understanding of PTMs in the intricate landscape of RNA-associated gene regulation.

Materials and methods

Plant growth conditions

In the experiments, we utilized wild-type *Arabidopsis thaliana* ecotype Col-0, *skb1-1* (SALK_065814; AT4G31120; N565814) and *tsn1/2* (from Sanchez-Coll Lab) mutant plants. Seedlings were grown on MS medium (pH 5.7) in growth cabinets under specific conditions: 50% humidity, 22–24°C, and a 16-hour-light/8-hour-dark regimen at 30 mEinstein m^{-2} s^{-1}. Protein expression analyses were conducted 10–14 days after germination. For inflorescence tissue, plants were grown in soil under the same light/dark regimen for three weeks. *Nicotiana benthamiana* RDR6 silenced plants (*rdr6i*) were maintained in growth chambers under long-day photoperiods, consisting of 16 h of light at 25°C and 8 h of darkness at 22°C.

Plasmid construction

To generate all constructs, we employed the pK7m34GW vector and multisite Gateway recombination (33). Promoters and coding sequences were amplified from Arabidopsis genomic DNA using Phusion polymerase (Thermo Scientific). These amplicons were then recombined into the corresponding pDONR plasmid using Gateway BP Clonase (Invitrogen). Similarly, fluorescent reporters were amplified, and all plasmids were sequenced for verification. Lastly, three-way recombination was performed using Gateway LR Clonase (Invitrogen) to generate the promoter:reporter-gene constructs utilized in this study.

Agrobacterium tumefaciens-mediated protein transient expression and stable transgenic lines generation

For protein transient expression assays in *rdr6i N. benthamiana*, binary vectors were introduced into *Agrobacterium tumefaciens* GV3101 through electroporation. The transformed bacteria were grown at 28°C in Luria-Bertani medium supplemented with the appropriate antibiotics. The bacterial cultures were collected and normalized to an OD600 of 0.15–0.5 using a solution containing 10 mM $MgCl_2$, 10 mM MES pH 5.6 and 150 μM acetosyringone. These suspensions were then infiltrated into the abaxial side of two-week-old *N. benthamiana* leaves. When simultaneous expression of two proteins was required, cultures containing the corresponding vectors were mixed prior to infiltration. Stable transgenic plants were generated using the floral dip method (34) in *A. thaliana* Col-0 wild-type and *skb1-1* mutant background plants. After floral dip, seeds were collected and selected on media containing antibiotics/herbicides to identify transformed individuals. Positive transformants were then grown, and subsequent generations were screened to confirm stable integration of the transgene.

Leptomycin B (LMB) treatment

For all experimental lines, five/eight-day-old seedlings were transferred to 3 ml of liquid MS medium (pH 5.7) and incubated for 24 h. Following this, LMB (Enzo Life Sciences) was added to a final concentration of 1 mM and incubated in darkness for 8–24 h.

Live cell imaging

To study subcellular localization, fluorescent protein reporter-expressing roots were imaged using a Zeiss Elyra 7 with Lattice SIM^2 immediately after excision from growing plants. Arabidopsis roots were prepared by mounting them in water and Propidium Iodide (PI). To visualize green fluorescent protein (GFP) and PI the 488 nm and 514 nm Diode laser were used for excitation. The fluorescence emitted from GFP was collected in the range of 492–532 nm, and that from PI was collected in the range of 590–615 nm, respectively. For Bimolecular Fluorescent Complementation (BiFC) assay, leaf disks of *N. benthamiana* were prepared by cutting and mounting them in water. For imaging yellow fluorescent protein (YFP) fluorescence and Cherry fluorescent protein (ChFP) fluorescence, the excitation was conducted using the 561 nm line of a laser for YFP and at 587 nm for ChFP, and emission signals were detected within the range of 530 nm for YFP and 610 nm for ChFP. The images presented in the figures are representative of consistent results obtained in at least three independent experiments. Image processing and analysis, including overlays were performed using FIJI software (35).

Protein immunoprecipitation

All steps were performed at 4°C/on ice. Inflorescences/seedlings from *A. thaliana*, or infiltrated leaves from *N. benthamiana* were frozen in liquid nitrogen and grounded using a pestle and mortar. The grounded tissue was mixed at a ratio of 1:3 with immunoprecipitation buffer (50 mM Tris–HCl, pH 7.5, 150 mM NaCl, 10% glycerol, 0.1% Nonidet *P*-40) supplemented with 10 μM proteasome inhibitor MG-132 (Merck) and complete protease inhibitor cocktail tablet (Roche). The mixture was incubated on a rotating wheel for 1 h at 4°C. Cell debris was removed by centrifugation twice at 12 000 g for 15 min. Protein levels of supernatants were determined using a colorimetric assay based on Bradford method (Bio-Rad Protein Assay Dye Reagent Concentrate, Bio-Rad) and normalized. For endogenous protein immunoprecipitations, the solution was precleared by incubating with Dynabeads™ Protein G (ThermoFisher Scientific) for 1 h at 4°C on a rotating wheel. The beads were then magnetically separated and removed. 20% of the supernatant was saved as the input control, and the remaining portion was incubated with the corresponding endogenous antibody (Supplementary Table S1) for 2 h at 4°C on a rotating wheel. Afterwards, Dynabeads were added to capture the protein associated with the antibody. For GFP-transgenic lines, the solution containing the normalized protein lysate was incubated with GFP-Trap Magnetic Agarose beads (ChromoTek) for 2 h at 4°C on a rotating wheel. Afterwards, beads were washed three times with immunoprecipitation buffer. Subsequently, they were resuspended in buffer of the same composition. The immuno-

precipitated protein was then released by boiling the samples at 95°C for 5 min using a protein loading buffer or pH elution following the manufacturer´s instructions (for endogenous @AGO2 and @AGO5).

Protein blot analysis

Proteins were resolved by SDS-PAGE and transferred to an Immobilon-P PVDF membrane (Millipore). After blocking for 1 h in 1× PBS + 0.1% Tween-20 supplemented with 0.05–5% non-fat dry milk, the membranes were incubated overnight at 4°C with constant shaking with primary antibodies (Supplementary Table S1). Subsequently, the membranes were washed three times in PBS + 0.1% Tween-20, followed by a 1 h incubation with horseradish peroxidase-conjugated goat anti-rabbit or anti-rat secondary antibodies (Supplementary Table S1). The membranes were then rinsed three times before detection using the ECL Super Bright Kit (Agrisera) and imaged using an Amershan IQ800 imaging system. Finally, the membranes were stained with Coomassie Brillant blue to serve as a loading control.

RNA extraction, RT-qPCR analysis and sRNA sequencing

Total RNA and RNA from IPs were extracted using TRIzol™ Reagent (Thermo Fisher-Scientific) following the manufacturer's instructions. For RT-qPCR analysis, Genomic DNA was removed from 1 μg RNA samples through DNase I (Thermo Scientific #EN0771) treatment. First-strand cDNA synthesis was conducted using RevertAid First-Strand cDNA synthesis kit (Thermofisher, #K1622). Subsequently, qRT-PCR analysis was performed using the Light Cycler detection system, Brilliant II SYBR® Green QPCR Master Mix, and the specific oligos (Supplementary Table S1). The specificity of oligonucleotides was ensured by Primer3Web 4.1.0 design, and their efficiency was evaluated via qRT-PCR using 10-fold serial dilutions of corresponding cDNA. For each biological sample, three biological replicates were analysed, each run-in technical triplicate. Expression levels were normalized using actin gene expression levels. For sRNA sequencing, sRNAs were processed into sequencing libraries using NEBNext SmallRNA Library Prep Set and then sequenced using the Novaseq6000 sequencer, both procedures were performed by Macrogen Korea.

Cell fractionation

1 g of 12-day-old Arabidopsis seedlings was ground to a fine powder in liquid nitrogen. The powder was resuspended in 5 ml grinding buffer (0.5 M Hexylene glycol, 10 mM $MgCl_2$, 5 mM β-mercaptoethanol, 20 mM MOPS pH 7 and complete protease inhibitor cocktail (Roche)) and filtered through a 40 μm cell strainer (Falcon). Drop by drop, Triton X100 was added up to a final concentration of 0.5% to the flow-through. The flow-through was centrifuged at 3500 rpm for 10 min at 4°C. The supernatant representing the cytoplasmic fraction was further centrifuged at 10000 g for 10 min at 4°C to remove any residual debris. The pellet from the 3500 rpm spin representing the nuclei was dissolved with 2 ml grinding buffer + 0.5% Triton X100 and loaded on top on a Percoll cushion made of 5 ml 30% Percoll (0.5 M Hexylene glycol, 10 mM $MgCl_2$, 5 mM β-mercaptoethanol, 20 mM MOPS pH 7, 30% Percoll and 0.5% Triton X100) and 2 ml 60% Percoll (0.5 M Hexylene glycol, 10 mM $MgCl_2$, 5 mM β-mercaptoethanol, 20 mM MOPS pH 7, 60% Percoll and 0.5% Triton X100). Percoll cushion was centrifugated 30 min at 400 g with a swing out rotor centrifuge to collect nuclei as a white pellet. The pellet was washed with 1 ml of grinding buffer + 0.5% Triton X100, and centrifuged at 3500 rpm for 10 min. The nuclear pellet was resuspended and boiled in 1× SDS loading buffer for 10 min for protein gel blot analysis.

Mass spectrometry (MS) analysis

For NTE^{AGO1} MS analysis, three biological replicates of 12-day-old seedlings were used. Beads used in immunoprecipitation were cleaned three times with 500 μl of 200 mM ammonium bicarbonate and 60 μl of 6 M urea/200 mM ammonium bicarbonate were added. Samples were then reduced with dithiothreitol (30 nmol, 37°C, 60 min), alkylated in the dark with iodoacetamide (60 nmol, 25°C, 30 min) and diluted to 1 M urea with 200 mM ammonium bicarbonate for trypsin (1 μg, 37°C) or chymotrypsin (1 μg, 25°C) digestion for 8 h. After digestion, the peptide mix was acidified with formic acid and desalted with a MicroSpin C18 column (The Nest Group, Inc.) before LC–MS/MS analysis. Samples were analyzed using an LTQ-Orbitrap Fusion Lumos mass spectrometer (Thermo Fisher Scientific, San Jose, CA, USA) coupled to an EASY-nLC 1200 (Thermo Fisher Scientific (Proxeon, Odense, Denmark). Peptides were loaded directly onto the analytical column and were separated by reversed-phase chromatography using a 50 cm column with an inner diameter of 75 μm, packed with 2 μm C18 particles. Chromatographic gradients started at 95% buffer A and 5% buffer B with a flow rate of 300 nl/min and gradually increased to 25% buffer B and 75% A in 52 min and then to 40% buffer B and 60% A in 8 min. After each analysis, the column was washed for 10 min with 100% buffer B. Buffer A: 0.1% formic acid in water. Buffer B: 0.1% formic acid in 80% acetonitrile. The mass spectrometer was operated in positive ionization mode with nanospray voltage set at 2.4 kV and source temperature at 305°C. The acquisition was performed in data-dependent acquisition (DDA) mode, and full MS scans with 1 micro scan at a resolution of 120000 were used over a mass range of m/z 350–1400 with detection in the Orbitrap mass analyser. Auto gain control (AGC) was set to 'standard' and injection time to 'auto'. In each cycle of data-dependent acquisition analysis, following each survey scan, the most intense ions above a threshold ion count of 10000 were selected for fragmentation. The number of selected precursor ions for fragmentation was determined by the 'Top Speed' acquisition algorithm and a dynamic exclusion of 60 s. Fragment ion spectra were produced via high-energy collision dissociation (HCD), normalized collision energy of 28%, and they were acquired in the ion trap mass analyser. AGC and injection time were set to 'Standard' and 'Dynamic', respectively, and an isolation window of 1.4 m/z was used. Digested bovine serum albumin (New England Biolabs cat #P8108S) was analysed between samples to avoid sample carryover and ensure the instrument's stability. QCloud (36) was used to control instrument longitudinal performance during the project. For data MS analysis, the acquired spectra were analysed using the Proteome Discoverer software suite (v2.5, Thermo Fisher Scientific) and the Mascot search engine (v2.6, Matrix Science (37)). The data were searched against an *Arabidopsis thaliana* (UP000006548) database, a list (38) of common contami-

nants, and all the corresponding decoy entries. For peptide identification, a precursor ion mass tolerance of 7 ppm was used for MS1 level, trypsin was chosen as enzyme, and up to three missed cleavages were allowed. The fragment ion mass tolerance was set to 0.5 Da for MS2 spectra. Monomethylation and dimethylation on arginine, oxidation of methionine, and N-terminal protein acetylation were used as variable modifications. In contrast, carbamidomethylation on cysteines was set as a fixed modification. False discovery rate (FDR) in peptide identification was set to a maximum of 1%. For the detection of NTE^{AGO1} interactors, NTE^{AGO1}-GFPGUS expressing plants were used as bait. Three biological replicates were performed and compared to $NTEm^{AGO1}$-GFPGUS used as a control. The confident preys were identified at the SaintExpress threshold 0.8 and above. For NTE^{AGO1} interactor enrichment comparison in Col-0 and *skb1-1* mutant plants, transgenic lines expressing *pAGO1:NTE^{AGO1}-GFPGUS* with similar protein levels of NTE^{AGO1}-GFPGUS in both Col-0 and *skb1-1* backgrounds were selected, and biological triplicates were co-immunoprecipitated. Spectral count data was normalized to the amount of GFPGUS in each sample and then, analysed using IPInquiry4 to retrieve fold changes and *P*-values for the volcano plot (39). For clustering, we used proteins with spectral counts only in one group and none in the other (arbitrarily assigning them a fold change of 6) and those with fold change >3. The curated list was fed into Cytoscape through the StringApp to retrieve enrichment data (40). The MCL algorithm was used for clustering, using all detected proteins as a background.

For AGO1 MS analysis, four biological replicates of plant inflorescences (4× biological replicates GFP-AGO1wt, 4x biological replicates GFP-AGO1_mNES, and 3× biological replicates Col-0) were used. IPs were performed as described above. The beads were pelleted by centrifugation and resuspended in 200 µl wash buffer. Proteins were eluted twice by adding 50 µl glycine (0.2 M pH 2.5) to the beads, vortexed for exactly 30 s, transferred to a fresh tube, and immediately neutralized by Tris-base (1 M, pH 10.4) for a final volume of 110 µl. The immunoprecipitation was validated by standard Western blot analysis and SDS-PAGE. The immunoprecipitated samples were analysed using proteolytic digestion and tandem mass spectrometry (LC/ESI/MS/MS). Results were visualized and analysed using Scaffold (Proteome Software). All proteins for which only one unique peptide was detected on the controls were eliminated for analysis. Parameters were set as follows: protein threshold: 99%, Min peptides: 2, peptide threshold: 99%.

The raw proteomics data have been deposited to the PRIDE (41) repository with the dataset identifier PXD049971.

Arginine methylation sites predictor

Arginine methylation site predictions were analyzed using Met-predictor (42). Met-predictor utilizes a support vector machine-based network that integrates a diverse range of sequence-based features derived from protein sequences with features based on predicted protein tertiary structure models.

3D Structure analysis

Structure prediction of Arabidopsis AGO1, AGO2, AGO3, AGO4 and AGO5 were conducted using ColabFold v1.5.2-patch (43), which integrates a simplified version of AlphaFold2 and Alphafold2-multimer. The alignment and templates were obtained using MMseqs2 and HHsearch. The Msa_mode employed was mmseqs2_uniref_env, and three recycles were performed for each model. Finally, five models were obtained for each AGO protein, with the best-ranked model being retained. For visualization purposes, the PyMOL™ Molecular Graphics System, Version 2.5.0, was utilized (44). The 3D structures data have been deposited to the ModelArchive repository with the accession codes ma-9tjqm, ma-5qyie, ma-plafl, ma-b22as and ma-r2taa.

Disorder amino acid sequence analysis

The disorder analysis was conducted using IUPRED3, standalone version, selecting 'long' as iupred_type, and the sequence was provided as input. The output provides the likelihood of disorder for each residue, represented as a score between 0 and 1, where values above 0.5 indicate disordered. Plots were generated using the matplotlib library in a Python script. Solvent accessibility was calculated using NACESS version 2.1.1, considering a probe of size 5, and utilizing the PDB file obtained with ColabFold as input.

Orthologues alignment and conservation

Alignments were performed using MEGA software (45) with the MUSCLE algorithm (46). Visualization and sequence conservation were achieved using ESPript 3, assigning a colour (in the grey scale) to a column based on whether the global score for each pair of sequences exceeded the SimilarityGlobalScore of 0.7. The conservation analysis for the putative methylated arginine residues and surroundings was conducted through a Python script.

Results

The amino-terminal extension of Arabidopsis AGO1 (NTE^{AGO1}) undergoes arginine methylation

The presence of GAR domains is significantly abundant in the NTEs of plant AGO1 proteins (Supplementary Figure S1A). To characterize them, we conducted bioinformatic analyses using Met-predictor, a tool that predicts lysine and arginine methylation sites based on a support vector machine (SVM) classifier (42), to identify potential methylation sites along the *A. thaliana* AGO1 protein, hereinafter referred to as AGO1. We identified ten arginine residues as candidates for methylation in the NTE (R6, R30, R34, R48, R59, R62, R83, R85, R94 and R101), one in the N-domain (R251), one in L1 (R361), and three in the C-terminal segment (CTE) (R1015, R1022 and R1025) of AGO1 (Figure 1A; Supplementary Table S2). Through disorder tendency prediction and structural modelling of AGO1 we found that while R251 and R361 are in structured and limited accessible regions, the remaining candidates are accessible and located in intrinsically disordered regions (Figure 1B; Supplementary Figure S1B, C; Supplementary Table S2).

To verify and validate these putative methylation sites, we initially immunoprecipitated the endogenous AGO1 protein. Subsequently, we examined its methylation status by western blot (WB) analysis, using a monoclonal antibody, which specifically detects sDMA. A strong signal was detected in the AGO1 protein purified from Arabidopsis wild-type plants (Figure 1C). To differentiate between the putative methylation sites located in the NTE (1–196AA) or the remaining parts of AGO1 (197–1050AA), we generated a

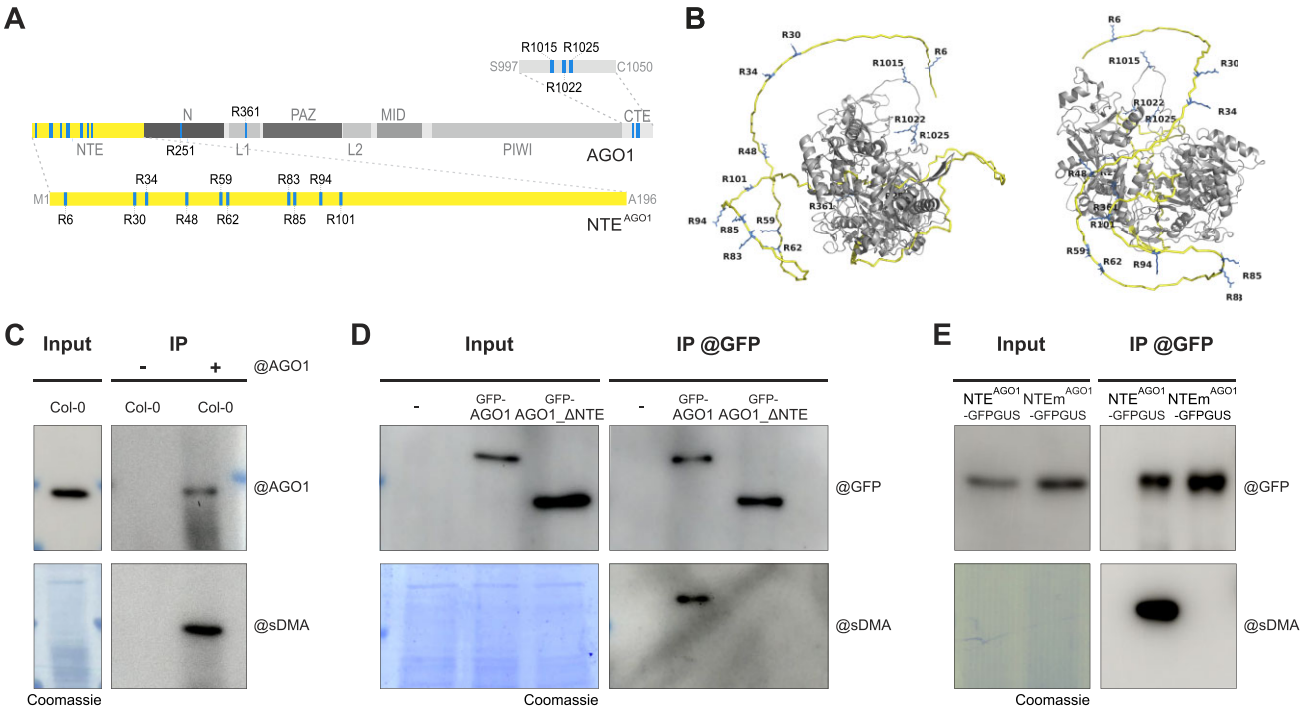

Figure 1. Arginine methylation of NTE^{AGO1} in *Arabidopsis thaliana*. (**A**) Schematic representation of putative arginine methylation sites predicted for AGO1. Globular domains are shown in grey, NTE in yellow and putative methylated arginine residues in blue. (**B**) Modelling views of AGO1 structure predicted using AlphaFold2. Globular domains are shown in grey cartoon, NTE in yellow cartoon and ribbon, and the putative methylated arginine residues in blue sticks. (**C-E**) Western blot assays showing methylation status of endogenous and transgenic versions of AGO1. Upon normalization of plant extracts by total content of protein, endogenous AGO1 was immunoprecipitated with anti-AGO1 antibody (C) and transgenic versions with anti-GFP magnetic agarose beads (D, E). Input and IP fractions were incubated with the corresponding antibody. IP fractions were also incubated with anti-sDMA antibody to test methylation status. Membranes containing input fractions were afterwards stained with Coomassie to serve as a loading control. All extracts were obtained from wild-type background (Col-0) plants. In (D), (-) refers to non-transgenic Col-0 plants. Transgenic versions of AGO1 fused to GFP or GFPGUS were cloned under the endogenous *AGO1* promoter. AGO1_ΔNTE: AGO1 lacking the NTE; NTE^{AGO1}: wild type NTE^{AGO1}; NTEm^{AGO1}: NTE^{AGO1} in which predicted R30, R34, R48, R59, R62, R83, R85, R94 and R101 putative methylated arginine residues were replaced by alanine residues.

shorter version of AGO1 where the NTE region was removed (AGO1_ΔNTE). AGO1_ΔNTE was fused to GFP (GFP-AGO1_ΔNTE) and expressed under the *AGO1* promoter in Arabidopsis. Immunoprecipitation (IP), followed by sDMA detection, revealed the absence of the detectable methylation signal in GFP-AGO1_ΔNTE, while the transgenic full-length version of GFP-AGO1 maintained a similar methylation status as the endogenous AGO1 (Figure 1D), suggesting that the NTE is primarily responsible for the sDMA signals in AGO1.

Next, we generated a fusion construct comprising the wild-type NTE fragment of AGO1 and GFPGUS (NTE^{AGO1}-GFPGUS) under the *AGO1* promoter, which we expressed in Arabidopsis. Similar to the full-length AGO1, the fusion protein containing the NTE^{AGO1} retained the sDMA signal (Figure 1E; Supplementary Figure S1D). Concurrently, to validate that the predicted arginine residues are indeed responsible for the sDMA signal, we generated a NTE^{AGO1} mutant fusion version where the arginine residues R30, R34, R48, R59, R62, R83, R85, R94 and R101 in the NTE were substituted by alanine residues (NTEm^{AGO1}-GFPGUS). It is worth noting that R6 has been described as part of a putative nuclear localization signal (14). Therefore, to prevent potential alterations in the subcellular localization of the NTE reporter that could affect PTMs, we opted not to mutate R6. We assessed the methylation status through IP followed by WB analysis. The absence of the sDMA signal was observed in the NTEm^{AGO1} version, as occurred in the GFPGUS controls, confirming the role of the nine arginine residues (or at least one of them) in the NTE^{AGO1} methylation (Figure 1E; Supplementary Figure S1D). Taken together, these results validate that the methylation in AGO1 is driven by exposed arginine residues exclusively located in its NTE.

PRMT5 interacts with NTE^{AGO1} and induces its methylation

While asymmetric arginine dimethylation is catalyzed by various PRMT proteins, PRMT5 emerged as the sole responsible for sDMA generation in Arabidopsis (47). To determine the enzyme responsible for AGO1 arginine methylation, we immunoprecipitated AGO1 from Arabidopsis transgenic lines expressing *pAGO1:GFP-AGO1*, and we analysed interacting proteins using mass spectrometry (MS) analysis. We identified 61 proteins exclusively associated with GFP-AGO1 but not detected in the wild-type control samples (Supplementary Table S3). Among the putative AGO1 interactors, we identified significant enrichment in PRMT5 (Figure 2A). Interestingly, we could identify the interaction of PRMT5 with the steady-state cytoplasmic wild-type version of GFP-AGO1 and the nuclear-only version of AGO1, in which point mutations were introduced in the nuclear export signal

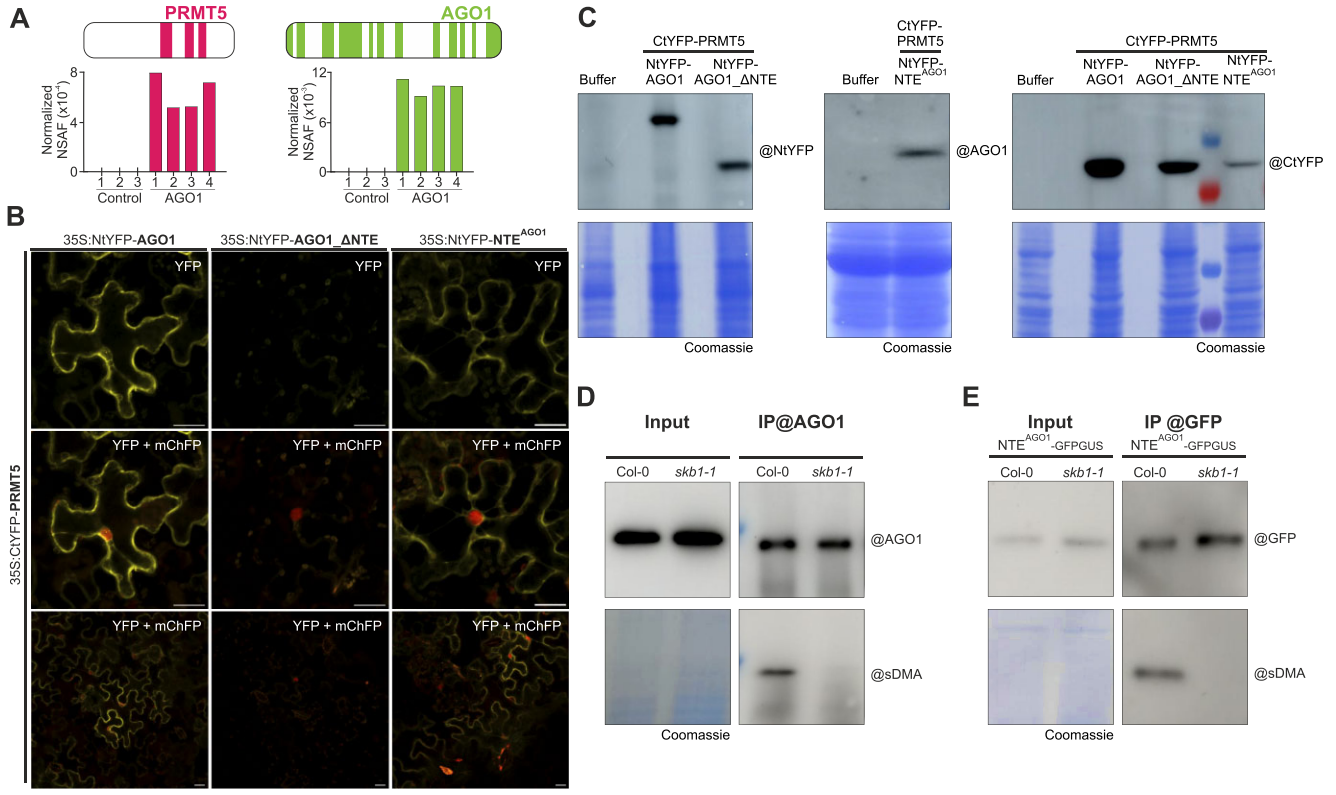

Figure 2. PRMT5 interacts and induces NTE^{AGO1} methylation. (**A**) Protein abundance estimates and sequence coverages of PRMT5 and AGO1 detected by mass spectrometry analysis of immunoprecipitated AGO1 from Arabidopsis plants expressing *pAGO1:GFP-AGO1*. Non-transgenic Arabidopsis plants have been used as a control. (**B**) Confocal images of Bimolecular Fluorescence Complementation (BiFC) assays showing the interaction between AGO1 and PRMT5 in *N. benthamiana* leaf cells. AGO1 versions and PRMT5 were tagged with the N-terminal (NtYFP-) or C-terminal (CtYFP-) parts of YFP, respectively, and expressed under the Cauliflower mosaic virus *35S* promoter. H2B-mCherry reporter was co-infiltrated as nuclear marker. The upper panels show the YFP channel. The middle and lower panels show YFP and mChFP merged channels (see also Supplementary Figure S2B). All images were taken three days after infiltration. Scale bars correspond to 25 μm. (**C**) Western blot assays showing expression levels of the tagged proteins. After SDS-PAGE, protein extracts from *N. benthamiana*' leaves used in the BiFC experiment shown in panel B were transferred to a PDVF membrane and incubated with anti-NtYFP or anti-CtYFP antibodies to confirm the expression of the Nt- and Ct- YFP tagged versions. Due to the no specificity of anti-NtYFP antibody at low molecular weight range proteins, the anti-AGO1 antibody (which recognizes the NTE of AGO1) was used to detect the expression of NtYFP-NTE^{AGO1}. Plants infiltrated with MES buffer were used as controls. Membranes were afterwards stained with Coomassie to serve as loading controls. (**D**, **E**) Western blot assays showing methylation status of endogenous AGO1 and transgenic NTE^{AGO1} in wild-type background (Col-0) and *prmt5 (skb1-1)* mutant background plants. Upon normalization of plant extracts by the total content of protein, endogenous AGO1 was immunoprecipitated with anti-AGO1 (D) while transgenic NTE^{AGO1} with anti-GFP magnetic agarose beads (E). Input and IP fractions were incubated with the corresponding antibody, and the IP fraction was also incubated with anti-sDMA antibody to test methylation status. Membranes containing input fractions were afterwards stained with Coomassie to serve as loading controls. AGO1_ΔNTE: AGO1 lacking the NTE; NTE^{AGO1}: wild type NTE^{AGO1}. NTE^{AGO1} fused to GFPGUS was cloned under the endogenous *AGO1* promoter.

(NES) of AGO1 (GFP-AGO1_mNES) to impair nuclear export (Supplementary Figure S2A) (14). This suggests that this interaction could occur either in the nucleus or cytoplasm.

The cytoplasmic and nuclear interaction between PRMT5 and AGO1, was then confirmed by Bimolecular Fluorescent Complementation (BiFC) assays in *Nicotiana benthamiana* leaves (Figure 2B; Supplementary Figure S2B, C). AGO1-PRMT5 interaction was also validated using the nuclear-only version of AGO1 (Supplementary Figure S2C). Notably, PRMT5 interaction was abolished upon deletion of the NTE^{AGO1} (AGO1_ΔNTE), but still present when NTE^{AGO1} was co-expressed with PRMT5 (Figure 2B; Supplementary Figure S2B), revealing that NTE alone was sufficient for the interaction with PRMT5. WB analyses showed comparable protein levels for all BiFC assays performed (Figure 2C; Supplementary Figure S2D). Altogether, this evidence firmly established the interaction of AGO1 with PRMT5 and emphasized the role of NTE in this interaction.

To study the role of PRMT5 in AGO1 symmetric arginine dimethylation, we conducted IP of endogenous AGO1 in wild-type background (Col-0) and *prmt5* mutant (mutant allele called *skb1-1*) Arabidopsis plants. *prmt5* mutant plants have diverse developmental abnormalities, such as growth retardation, smaller cotyledons, rosette leaves and primary roots, and delayed flowering time. Furthermore, PRMT5 has been suggested to impact plant fertility, yet the precise molecular mechanisms responsible for these effects remain poorly understood (48). Subsequent WB analysis confirmed the lack of symmetric arginine dimethylation of the endogenous AGO1 in the *skb1-1* mutant background (Figure 2D). Similar results were obtained using *pAGO1:NTE^{AGO1}-GFPGUS* transgenic Arabidopsis lines, thereby confirming that NTE^{AGO1} is recognized and methylated by PRMT5 (Figure 2E). Collectively, these findings provide robust evidence supporting the role of PRMT5 and the NTE^{AGO1} during AGO1 symmetric arginine methylation.

The R48-R85 region of the NTE^{AGO1} is responsible for PRMT5-dependent methylation

Following confirmation of PRMT5-mediated methylation of NTE^{AGO1}, our objective was to pinpoint the methylated arginine residues (49). IP coupled to MS (IP-MS), conducted using the full-length GFP-AGO1, covered only ∼28% of the NTE^{AGO1} (Figure 2A; Supplementary Figure S3A). To improve coverage of the NTE^{AGO1}, we conducted IP-MS using NTE^{AGO1} fused to GFPGUS under the *AGO1* promoter. Additionally, we employed a combination of two proteolytic enzymes (trypsin and chymotrypsin) and two genetic backgrounds (wild-type and *skb1-1*), with at least three biological replicates per condition (Figure 3A). This strategy allowed us to generate complementary proteolytic profiles, significantly enhancing protein coverage and identifying modified residues. For example, in arginine-rich domains, trypsin tends to generate short and highly polar peptides that pose challenges for separation and sequencing. In contrast, chymotrypsin yields peptides more amenable to MS analysis. Moreover, utilizing the *skb1-1* mutant background enabled the identification of distinct fragmentation data, as trypsin cleaves not methylated arginine residues. Furthermore, employing the *skb1-1* mutant plants allowed us to confirm arginine methylations exclusively dependent on PRMT5.

After MS analyses, we achieved 87% sequence coverage for the NTE^{AGO1} region (170/196AA) (Figure 3A, Supplementary Figure S3B). We identified five arginine residues (R5, R6, R20, R112 and R182) consistently unmethylated in wild-type background plants (Figure 3B, C). While R5, R20, R112 and R182 were already predicted as not methylated sites (Figure 1A), we also confirmed that R6 remained unmethylated *in vivo*, contrary to the Met-predictor prediction (Supplementary Table S2). Moreover, six arginine residues (R30, R34, R62, R85, R94 and R101) remained dimethylated in the *skb1-1* mutant plants, suggesting the involvement of other PRMT proteins in NTE^{AGO1} methylation, which implies that AGO1 could also undergo aDMA modification (Figure 3B, C; Supplementary Table S2). However, MS analysis limitations hindered the definitive determination of whether these six arginine residues are asymmetrically dimethylated in wild-type plants or if PRMT5 absence leads to aDMA production by others PRMT proteins (type I). Further studies are required to address this question. More importantly, three arginine residues (R48, R59 and R83) showed methylation dependency on PRMT5. R48 and R83 were methylated in wild-type and unmethylated in *skb1-1* mutant background plants, confirming their PRMT5 dependency. R59 was undetected in *skb1-1* mutant and wild-type background plants. However, MS-detected peptides exhibited trypsin cleavages occurring at R59 exclusively in *skb1-1*, suggesting possible PRMT5-dependent methylation (Figure 3B, C; Supplementary Figure S3C, Supplementary Table S2). Despite variability in other NTE regions, sequence studies on AGO1 orthologs across diverse plant species highlight strong conservation, particularly in R48, R59 and R83, suggesting an evolutionary role for these symmetric and asymmetric dimethylated arginine residues (Figure 3D; Supplementary Figure S3D).

To validate the contribution of each arginine residue, we generated Arabidopsis transgenic lines expressing specifically distinct segments of the NTE^{AGO1} containing different arginine residues: NTE^{AGO1} (M1-A196), NTE-L (M1-Q111), NTE-R (Q111-A196), NTE-L1 (M1-Q55), NTE-L2 (Q55-Q111), NTE-L2a (Q55-Q81) and NTE-L2b (Q81-Q111) (Figure 3E). Each segment was fused to GFPGUS, expressed in Arabidopsis plants under *AGO1* promoter and immunoprecipitated. After standardizing protein amounts for the seven IPs we observed that NTE-L was the primary contributor to methylation (Figure 3F). Interestingly, the deletion of the Q111-A196 segment, devoid of any methylation sites, led to a significant reduction in the sDMA signal in comparison with NTE, indicating a crucial role during AGO1 methylation (Figure 3F). The decrease in methylation levels as the segments decreased in size was also found when we compared NTE-L1 and/or NTE-L2 levels versus NTE-L (Figure 3F). To overcome this challenge based on the size of the fragment, we specifically compared the pairs NTE-L versus NTE-R, NTE-L1 versus NTE-L2, and NTE-L2a versus NTE-L2b using higher protein amounts (Figure 3G; Supplementary Figure S3E). Results confirmed arginine methylation accumulation in NTE-L, particularly in NTE-L2, where R59 and R83 were initially identified (Figure 3G). Remarkably, we could not detect any signal in NTE-L2a versus NTE-L2b at higher protein levels (Supplementary Figure S3E), suggesting that either a minimum of two arginine residues are required synergistically for WB detection, or PRMT5 might require a larger segment for effective recognition and methylation of arginine residues. Overall, MS and WB data suggest that NTE^{AGO1} undergoes symmetric and asymmetric arginine dimethylation, being the R48-R85 region primarily responsible for the PRMT5-dependent methylation.

Symmetric arginine dimethylations do not affect AGO1 subcellular localization

Previous studies have described that arginine methylation can influence the subcellular localization of specific proteins. Thus, we aimed to investigate whether the lack of symmetric arginine dimethylation in AGO1 could impact its nucleo-cytosolic shuttling capabilities (14). Our analyses revealed that NTE^{AGO1} contains both sDMA and aDMA. Since sDMA and aDMA can generate opposite biological effects (50), instead of introducing a point mutation on AGO1 which will abolish both types of methylation therefore possibly hiding aDMA effects, we chose to study AGO1 nucleo-cytosolic shuttling capabilities in the absence of PRMT5, ensuring the absence of only sDMA. To explore whether sDMA could influence AGO1 subcellular localization, we generated full-length AGO1 fused to GFP expressed under *AGO1* promoter in both Arabidopsis wild-type background and *skb1-1* mutant plants, and we analysed them under confocal microscopy. The absence of PRMT5 did not alter the previously observed cytosolic steady-state localization of GFP-AGO1 (Figure 4A; Supplementary Figure S4A, B). Subsequently, to examine the transient nuclear subcellular localization of GFP-AGO1 in these two lines, we treated them with Leptomycin B (LMB), a well-established nuclear export inhibitor. Nuclear localization of GFP-AGO1, after LMB treatment, remained comparable in wild-type and *skb1-1* mutant background plants (Figure 4A; Supplementary Figure S4A, B). Cell fractionation followed by WB confirmed confocal analysis (Supplementary Figure S4C). Furthermore, to overcome the limited drug penetrance and eliminate any potential secondary consequences of the LMB treatment (such as those caused by other nuclear-shuttling proteins affected by LMB or the stress produced due to drug

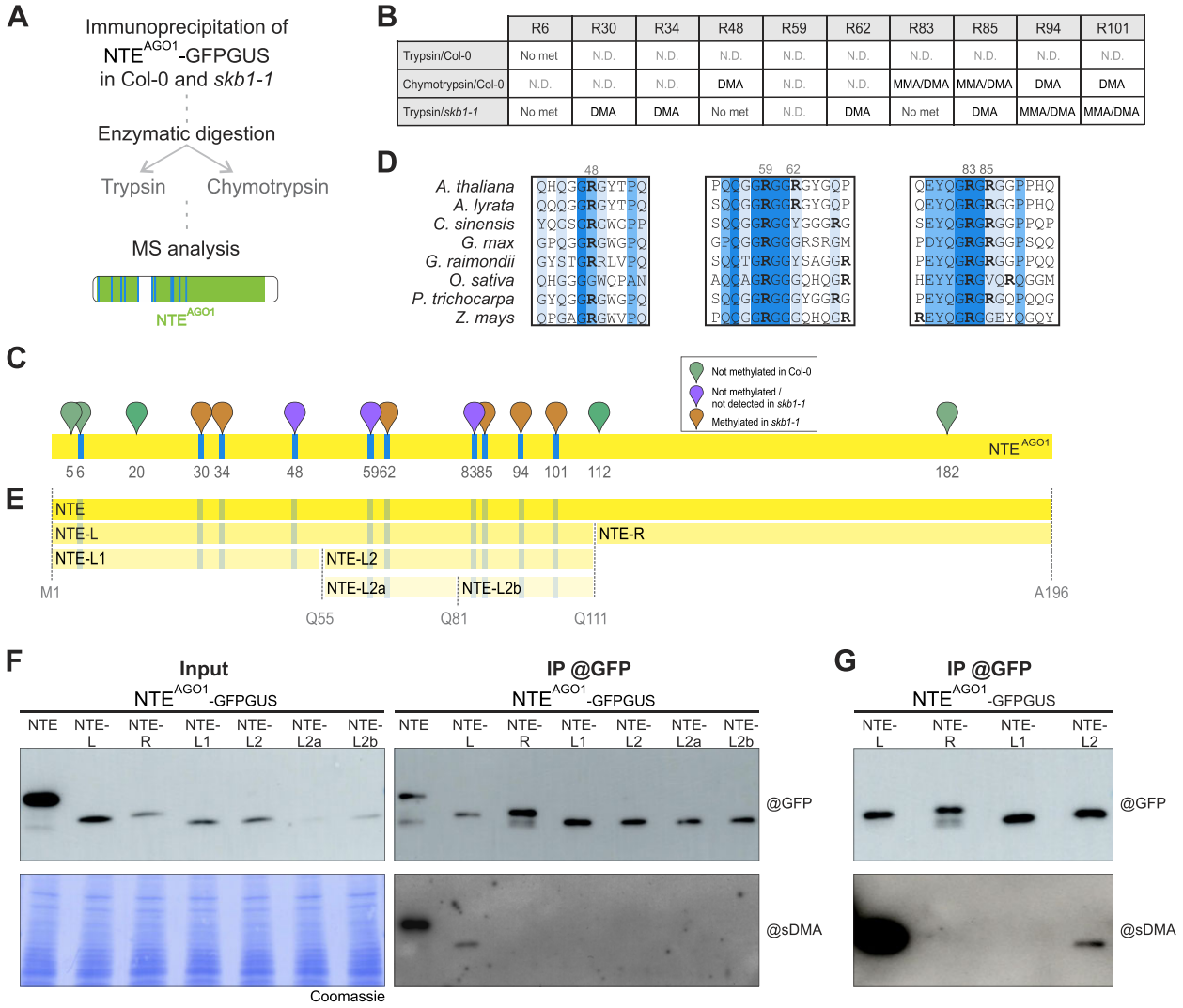

Figure 3. Identification of specific PRMT5-mediated methylation sites in NTE^{AGO1}. (**A**) Schematic representation of the strategy employed to analyse arginine methylation sites in NTE^{AGO1} by mass spectrometry (MS). The coverage of NTE^{AGO1} amino acid sequence detected is highlighted in green. Putative methylated arginine residues are highlighted in blue. (**B**) Table summarizing the methylation status of the different arginine residues (R6, R30, R34, R48, R59, R62, R83, R85, R94 and R101) found by MS analysis of immunoprecipitated NTE^{AGO1} after trypsin (wild-type background (Col-0) and *prmt5* background (*skb1-1*)) or chymotrypsin (Col-0) treatment. MMA: arginine monomethylation; DMA: arginine dimethylation; No met: no-methylation detected; N.D.: no coverage of arginine detected (see Supplementary Figure S3C for trypsin cleavage sites detected). (**C**) Schematic representation of the methylation status of arginine residues detected by MS. Green: not methylated in Col-0, purple: not methylated/not detected in *skb1-1*, orange: methylated in *skb1-1*. (**D**) AGO1 regions holding methylatable arginine residues were locally aligned with AGO1 orthologs from other plant species using MEGA with MUSCLE algorithm. Conservation is represented by a colour gradient (from highly conserved residues in blue to poorly conserved in white). *A. thaliana: Arabidopsis thaliana; A. lyrate: Arabidopsis lyrate; C. sinensis: Citrus sinensis; G. max: Glycine max; G. raimondii: Gossypium raimondii; O. sativa: Oryza sativa; P trichocarpa: Populus trichocarpa; Z. mays: Zea mays.* (**E**) Schematic representation showing the length of the different NTE^{AGO1} fragments used in sections F-G: NTE^{AGO1} (M1-A196), NTE-L (M1-Q111), NTE-R (Q111-A196), NTE-L1 (M1-Q55), NTE-L2 (Q55-Q111), NTE-L2a (Q55-Q81), and NTE-L2b (Q81-Q111). (**F**, **G**) Western blot assays showing methylation status of specific regions of NTE^{AGO1}. After normalization of plant extracts by the total content of protein, the seven versions of the NTE^{AGO1} fused to GFPGUS were incubated and immunoprecipitated with anti-GFP magnetic agarose beads. Input and IP fractions were incubated with anti-GFP antibody, and the IP fractions were also incubated with anti-sDMA antibody to check methylation status. Membrane containing input fractions was afterwards stained with Coomassie to serve as the loading control. All transgenic versions of NTE^{AGO1}-GFPGUS were cloned under the endogenous *AGO1* promoter and expressed in Col-0 plants.

treatment), we introduced the nuclear-only version of AGO1 fused to GFP (GFP-AGO1_mNES) into wild-type background and *skb1-1* mutant plants. Consistent with the observations of GFP-AGO1 treated with LMB, GFP-AGO1_mNES reporters exhibited the same subcellular localization in both wild-type background and *skb1-1* mutant plants (Figure 4A; Supplementary Figure S4A, B). However, these studies cannot exclude the possibility that in the absence of sDMA, aDMA may still play redundant functions in regulating AGO1 subcellular localization pattern. Altogether, results showed that in the absence of symmetric arginine dimethylation, AGO1 has a cytoplasmic steady-state and nuclear transient subcellular localization, indicating the protein exhibited the same shuttling mechanisms.

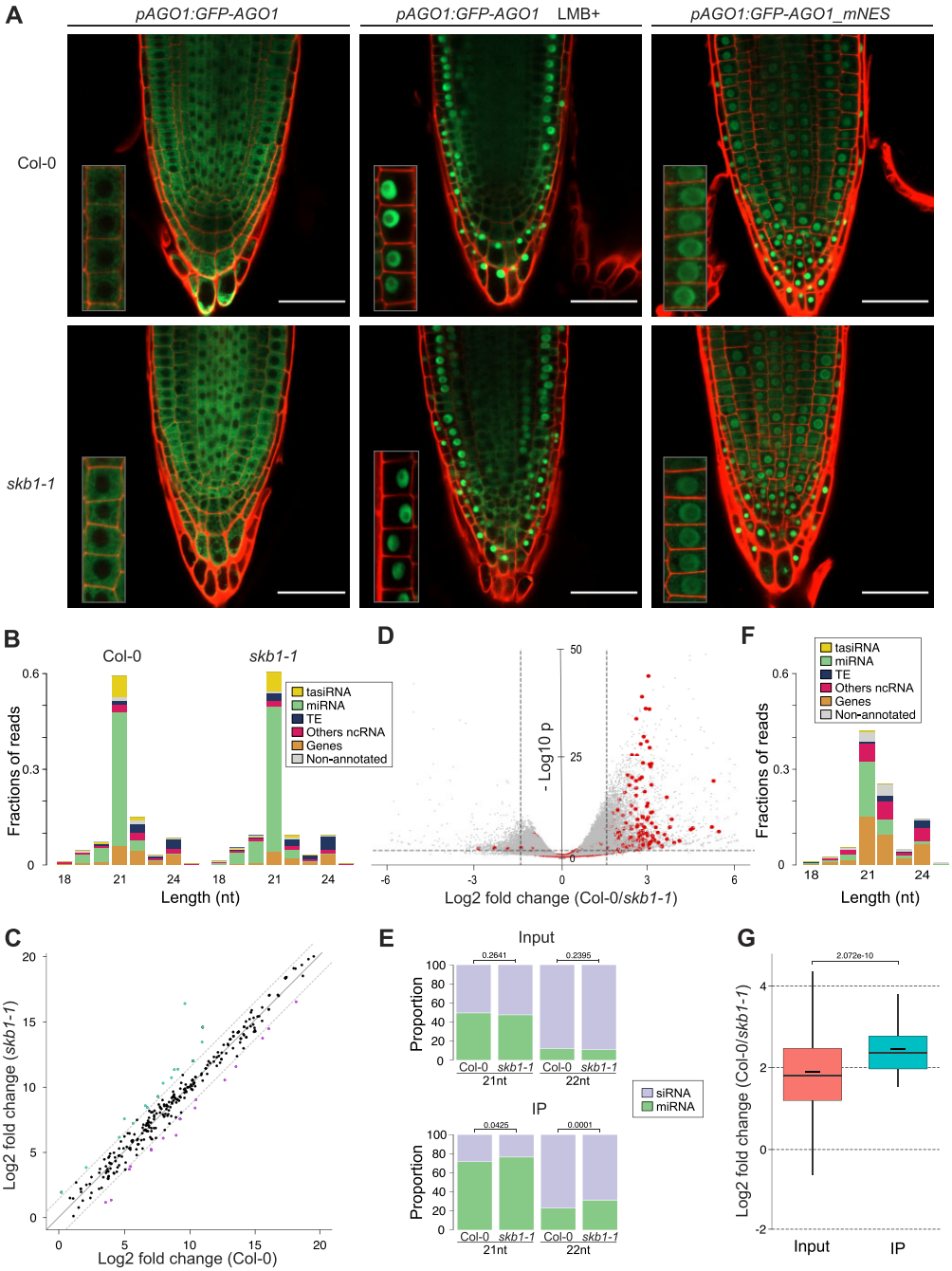

Figure 4. Implication of PRMT5 in AGO1's subcellular localization and sRNA loading. (**A**) Confocal images of wild-type background (Col-0) and *prmt5* (*skb1-1)* mutant background plants showing AGO1 subcellular localization. Roots from transgenic lines expressing *pAGO1:GFP-AGO1* were analysed under normal conditions and Leptomycin B (LMB+) treatment (left and middle panels, respectively). Roots from transgenic lines expressing *pAGO1:GFP-AGO1_mNES* under normal conditions are also shown (right panels). Bottom-left insets show magnification of 4–6 epidermal cells (for whole photos see Supplementary Figure S4B). Propidium iodide fluorescence is shown in red. Scale bars correspond to 50 μm. (B–G) Analysis of the RNA sequencing data obtained from input and AGO1 IP fractions from Col-0 and *skb1-1* mutant plants. Three biological replicates of each genotype were included in the analysis. (**B**) Size distribution of total sRNAs extracted and sequenced from IP fractions. Colours represent the identity (genomic source) of the sRNAs: miRNAs (green), tasiRNAs (yellow), protein-coding genes (orange), transposons/repeats (blue), non-annotated regions (grey) and other ncRNA (including transfer/ribosomal/small nuclear/small nucleolar RNAs) (pink). (**C**) Scatter plots comparing the $\log_2$ of the means of three biological replicates of miRNA co-immunoprecipitated with AGO1. The central line represents a $\log_2$ fold change of 0, and the dashed lines correspond with $\log_2$ fold change >1.5 and <1.5. Magenta dots represent the miRNAs enriched in Col-0 plants, and aquamarine dots represent the miRNAs enriched in *skb1-1* mutant plants. (**D**) Volcano plot representing the sRNAs differentially loaded in AGO1 in Col-0 and *skb1-1* mutant plants. Each dot corresponds with a window of 100nt generated along the Arabidopsis genome. Dots highlighted in red are windows containing RDR6-dependent sRNA. The horizontal dashed line represents the threshold of the adjusted *P*-value (0.05) and the vertical, the $\log_2$ fold change of 1.5. (**E**) Proportion of 21nt and 22nt miRNA and siRNA sequenced from input and IP fractions. *P*-adj values shown were calculated using *t*-test. (**F**) Size distribution of the sRNA enriched in Col-0 (depleted in *skb1-1* mutant plants). Colours represent the identity of sRNAs as in section B. (**G**) Boxplot representing the log2 fold change in the *skb1-1* mutant compared to Col-0 plants of the sRNA RDR6-dependent that were found to be depleted in IP fractions of *skb1-1* mutant plants. On the left, in pink are plotted the values of $\log_2$ fold change of windows from input fractions. On the right, in blue the $\log_2$ fold change of the same windows from IP fractions. Wilcoxon test was applied, and the adjusted *P*-value is shown above the boxes.

While the global miRNA loading into AGO1 exhibits minimal changes, a subset of siRNA is depleted in *skb1-1* mutant plants

Arginine methylation can profoundly influence protein-nucleic acid interactions, a phenomenon that aligns with the fact that over 60% of methylated arginine residues are located within proteins interacting with RNA. Recently, the indispensable role of the NTE in the miRNA loading activity of AGO1 was revealed (15). To explore the influence of NTE methylation on the sRNA loading activity of AGO1, we compared the sRNA cargoes of AGO1 in wild-type and *skb1-1* mutant plants. We conducted endogenous AGO1 IP from the inflorescences of three biological replicates from both backgrounds followed by sRNA sequencing analysis (Supplementary Figure S5A). Consistent with published results from AGO1 IPs from wild-type plants (51), the most abundant sRNA cargoes were 21nt-long miRNAs (Figure 4B). Remarkably, sRNA cargoes of AGO1 immunoprecipitated from *skb1-1* mutant plants showed comparable sizes and classes (genomic source of the generated sRNA) as wild-type plants (Figure 4B). Additionally, sRNA cargoes immunoprecipitated from AGO1 from *skb1-1* mutant plants also exhibited the typical uracil bias found in the 5′nt of sRNA loaded in AGO1 in wild-type plants (Supplementary Figure S5B). Differential analysis showed that most miRNA (∼90%) were equally distributed in AGO1 immunoprecipitated from wild-type and *skb1-1* mutant plants (Figure 4C; Supplementary Table S4). Only a few miRNAs showed significant quantitative variations ($\log_2$ fold change > 1.5), showing opposite behaviour. While 18 miRNAs of 326 TAIR-annotated were found to be enriched in AGO1 in wild-type plants, 35 were enriched in AGO1 in *skb1-1* mutant plants (Figure 4C; Supplementary Table S4). Among these differentially loaded miRNAs, we found no sequence bias for up- or down-regulated loading into AGO1. These results suggest that the loading of miRNA into AGO1 is not globally affected in the absence of PRMT5.

In addition to miRNA, ∼30% of the sRNA loaded in AGO1 corresponds to siRNAs. While miRNAs are produced from stem-loop in the nucleus, siRNAs are commonly generated (in the nucleus and the cytoplasm) from dsRNA with multiple origins, such as RNA-dependent RNA polymerase (RDR) products, long inverted repeats, natural antisense genes, or intergenic regions (52). To study siRNA loading into AGO1, we analysed differentially loaded siRNA by generating windows of 100nt along the Arabidopsis genome. We found 4494 windows producing sRNA differentially loaded in AGO1 immunoprecipitated from wild-type and *skb1-1* mutant plants (3174 enriched in wild-type and 1320 enriched in *skb1-1* mutant plants) (Figure 4D; Supplementary Table S5). Using RNA sequencing (RNAseq) we ruled out an indirect effect of the lack of PRMT5 on the transcription of these genes. Additionally, we conducted sRNA sequencing on biological triplicates of the input fractions. The siRNAs abundance relative to miRNA was comparable between wild-type and *skb1-1* mutant plants. However, in the IP fractions, we observed a depletion of siRNAs, particularly 22nt, in *skb1-1* mutant plants (Figure 4E; Supplementary Figure S5C). While the nature of the sRNA enriched in AGO1 IP in *skb1-1* mutant plants showed similar sizes and genomic annotations as typical sRNAs immunoprecipitated with AGO1 from wild-type plants (Supplementary Figure S5D), the sRNA enriched in AGO1 IP in wild-type plants (depleted in *skb1-1* mutant plants) showed clear enrichment in 21–22nt siRNA originating from protein-coding genes, resembling siRNA generated from RDR dependent dsRNA (Figure 4F). Remarkably, 55 of the 183 (30%) previously described RDR6-dependent siRNA producers genes were represented in the sRNA-depleted *skb1-1* mutant plants (Figure 4D; Supplementary Table S5).

The levels of sRNAs could be influenced by their loading into AGO proteins. If a particular sRNA is loaded more efficiently, it becomes protected from degradation, which leads to its increased abundance within the cell. As a result, there is usually a consistent correlation between differentially loaded sRNAs and their representation in the overall sRNA population, making it difficult to differentiate biogenesis or loading effects. To investigate these RDR6-dependent siRNA differentially loaded siRNAs, we analysed siRNA levels in biological triplicates of the input fractions of wild-type and *skb1-1* mutant plants, and we compared them to those obtained from IP fractions. The results revealed significant enrichment in the $\log_2$ fold change wild-type/*skb1-1* of these siRNAs in the IP fractions compared to the input fractions, suggesting that the loading per se, rather than the biogenesis of these siRNAs, is primarily responsible for this differential accumulation (Figure 4G). Simultaneously, to rule out any indirect effect of the absence of PRMT5 in the accumulation of the mRNAs main producers of the differentially loaded siRNAs, we measured their levels by qPCR in wild-type and *skb1-1* mutant plants. No significant changes were detected in any of them (Supplementary Figure S5E). Altogether, these results confirm that the loading of these siRNAs is affected in *skb1-1* mutant plants, minimizing the possibility of any indirect effect due to the levels of the mRNA substrates or siRNA biogenesis. These analyses collectively demonstrate that while global AGO1 miRNA loading exhibits minimal changes, some siRNAs, in particular 22nt-long, were specifically depleted in *skb1-1* mutant plants.

Lack of PRMT5 causes drastic reshaping of NTE^{AGO1} interactome

Recent studies have demonstrated that NTE^{AGOs} could serve as flexible platforms promoting protein-protein interactions (16). To investigate whether the arginine methylation occurring in NTE^{AGO1} affects its potential protein interactors, we conducted NTE^{AGO1} IP/MS using Arabidopsis plants expressing NTE^{AGO1} fused to GFPGUS under the *AGO1* endogenous promoter (*pAGO1:NTE^{AGO1}-GFPGUS*). Leveraging the intrinsically disordered nature of the NTE, we opted for this methodology to enhance the detection of potential proteins interacting with the methylated arginine residues while minimizing the high number of false positives typically observed in full-length AGO1 proteins IPs. As a negative control, we used Arabidopsis transgenic plants expressing *pAGO1:NTEm^{AGO1}-GFPGUS*, which allowed us to enrich interacting proteins that are dependent on the presence of the putative methylation sites. As a result, we have identified a small number ($n = 9$) of proteins statistically significant (Supplementary Table S6). At the same time, by examining proteins that exclusively interact with NTE^{AGO1} but are absent in NTEm^{AGO1}, albeit these findings were not statistically significant, we identified a few PRMT5 peptides. This finding endorses the BiFC assay previously described (Figure 2B), which revealed that NTE^{AGO1} alone is capable of interacting with PRMT5 (Supplementary Table S6). The interaction be-

tween NTE^{AGO1} and PRMT5 appears to be weaker compared to that of full-length AGO1, as evidenced by the lower number of detected peptide counts. Additionally, we detected a few peptides of TSN2 (Supplementary Table S6). Tudor proteins have been identified as the main reader of sDMA motifs in eukaryotic organisms. Gutierrez-Beltran et al., identified AGO1 as an interactor of TSN1 and TSN2, the two TUDOR proteins in Arabidopsis, under stress and non-stress conditions (53). To provide robust confirmation, we conducted a co-IP assay in Arabidopsis with an antibody that recognizes AGO1, and a serum to detect TSN1/TSN2 proteins. We could effectively validate these interactions *in vivo* in Arabidopsis (Figure 5A).

To better elucidate how specifically sDMA affects NTE^{AGO1} interactome, we also analysed putative protein interactors of NTE^{AGO1} in *skb1-1* mutant background plants. Transgenic lines expressing *pAGO1:NTE^{AGO1}-GFPGUS* with similar protein levels of NTE^{AGO1}-GFPGUS in both wild-type and *skb1-1* backgrounds were selected, and biological triplicates were co-immunoprecipitated. Proteins were identified by MS, and the changes in the abundance of pulled-down interactors under these two conditions were quantified (Figure 5B; Supplementary Table S7). As a result, we have discovered a small number of proteins preferentially interacting with NTE^{AGO1} in wild-type background plants. On the other hand, we identified a high number of proteins preferentially interacting with NTE^{AGO1} in *skb1-1* mutant plants (Supplementary Table S7). Interestingly, several of the interactors of NTE^{AGO1} in *skb1-1* mutant plants belong to major RNA-related functional clusters, such as mRNA splicing proteins (5% of the interactors), RNA Pol II complex (2.5%), Protein stabilization (2%), and Protein translation (2%) (Figure 5C; Supplementary Table S7). Additionally, various proteins related to AGO1 functions such as CLP1, SE, STA1, and UPF1 preferentially interact with NTE^{AGO1} in the *skb1-1* background (Supplementary Table S7). Interestingly, three PRMTs (PRMT1A, PRMT1B, PRMT10) were detected among the protein interactors identified within NTE^{AGO1} in *skb1-1* mutants but absent in wild-type background plants (Table S7). This finding could hold significance in the context of AGO1 arginine methylation, implying that in the absence of sDMA, alternative methylation types, such as MMA or aDMA, may potentially occur in the protein. Taken together, these results suggest that the presence of PRMT5 drastically reshapes NTE^{AGO1} interactome, specifically increasing the number of interactors of NTE^{AGO1} when PRMT5 is absent.

NTE symmetric arginine dimethylation is a common process in Arabidopsis AGO1, AGO2, AGO3 and AGO5

Although plants lack PIWI subfamily proteins, they have diversified sRNA functions in a consortium of several AGO proteins. Following the validation of sDMA methylation on AGO1, we conducted the same bioinformatic analyses to identify potential arginine methylation in all Arabidopsis AGO proteins. In addition to AGO1 and the previously reported AGO2 (32), AGO3 and AGO5 displayed significant numbers of GAR domains (Supplementary Figure S6A, B). Similar to AGO1, most of the predictions were associated with arginine residues located in intrinsically disordered and exposed NTEs of each protein (AGO1: 10 of 15; AGO2: 18 of 20; AGO3: 36 of 40; and AGO5: 12 of 17) (Figure 6A, B; Supplementary Table S2; Supplementary Figure S6C, D). Remarkably, none of the four AGO proteins involved in TGS (AGO4, 6, 8 and 9) showed significant numbers of putative exposed methylation sites. Sequence alignments showed high conservation among putative methylation sites predicted in AGO5 and those validated in AGO1 (both located in Clade I), particularly in the case of AGO1 R48, and the regions R59–62 and R83–85 (Supplementary Figure S6E). Additionally, they display strong conservation among different AGO5 orthologs from several plant species (Supplementary Figure S6F). Similar conservation patterns were observed among methylation sites predicted in AGO3 and AGO2 (Supplementary Figure S6G).

To validate these predicted PTMs, we initially transiently overexpressed NTE^{AGO1}, NTE^{AGO2}, NTE^{AGO3} and NTE^{AGO5}, fused to GFPGUS under the *35S* promoter in *N. benthamiana* leaves. Negative controls included the overexpression of GFPGUS alone and NTE^{AGO4} fused to GFPGUS. The NTE constructs were then immunoprecipitated, and their positive methylation status was confirmed by WB analysis for NTE^{AGO3} and NTE^{AGO5}, as well as expected, for NTE^{AGO1} and NTE^{AGO2} (Figure 6C). Remarkably, NTE^{AGO3} showed the highest ratio sDMA signal per protein quantity, while NTE^{AGO5} displayed the lowest one. Interestingly, a side-by-side comparison also suggests that AGO1 shows a higher sDMA signal per protein quantity than AGO2 (Figure 6C).

To further validate AGO3 and AGO5 arginine methylation in Arabidopsis, we conducted IP from wild-type plants. We could confirm the presence of sDMA in endogenous AGO5, and in endogenous AGO2, used as a control (Figure 6D). However, we encountered technical limitations with anti-AGO3 antibodies preventing us from performing endogenous IP for AGO3. To overcome this, we utilized Arabidopsis transgenic plants expressing *pAGO3:NTE^{AGO3}-GFPGUS* construct. *pAGO2:NTE^{AGO2}-GFPGUS* was used as positive control. Results validated AGO3 methylation *in vivo*. In addition, in agreement with the results observed in *N. benthamiana* NTE^{AGO3} showed a stronger sDMA signal per protein quantity than NTE^{AGO2} at the same membrane exposition times (Figure 6E) suggesting that NTE^{AGO3} is strongly targeted for sDMA *in vivo*. In summary, our findings confirm that the NTE of AGO1, AGO2, AGO3 and AGO5, undergo symmetric arginine dimethylation. Moreover, we demonstrate that these methylation sites exhibit conservation among members of the same clade and AGO orthologs from diverse plant species. The shared presence of predicted arginine methylation sites within their NTEs suggests a broader and unified regulatory mechanism across AGO protein family.

Discussion

In animals, arginine methylation of NTE from PIWI proteins plays a crucial role in regulating their biological functions (29–31). In Arabidopsis, previous studies have highlighted the indispensable nature of the NTE for various AGO1 functions, including ER membrane association, nuclear shuttling, sRNA loading, and protein interaction (13–16). Our study reveals that NTE^{AGO1} undergoes symmetric arginine dimethylation at specific residues and interacts with the methyltransferase PRMT5, which catalyzes its methylation. Additionally, we also demonstrated that symmetric arginine dimethylation also occurs in NTE^{AGO3} and NTE^{AGO5} (as was previously described for AGO2 (54)) indicating a conserved role of the

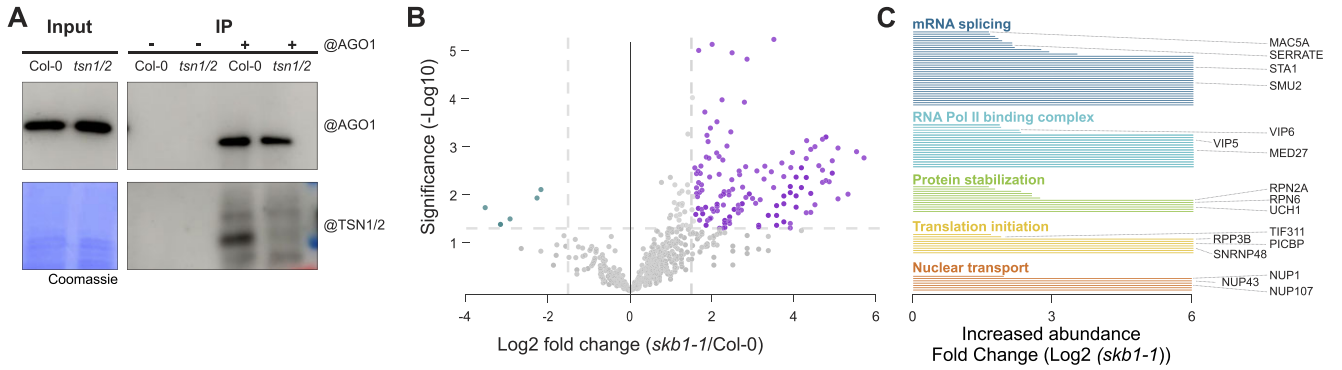

Figure 5. PRMT5-driven remodelling of NTE^{AGO1} interactome. (**A**) Western blot assay of input and AGO1 IP fractions showing the interaction between AGO1 and TSN1/2. After normalization of plant extracts obtained from wild-type background (Col-0) and *tsn1/2* mutant plants by the total content of protein, the endogenous AGO1 was immunoprecipitated with anti-AGO1 antibody. Input and IP fractions were incubated with anti-AGO1 antibody. IP fraction was also incubated with an anti-TSN1/2 serum to check the interaction between both proteins. Membrane containing input fractions was afterwards stained with Coomassie to serve as loading control. (**B**) Volcano plot representing proteins that were found enriched interacting with NTE^{AGO1}-GFPGUS in *prmt5* (*skb1-1)* mutant background plants (in purple) compared to NTE^{AGO1}-GFPGUS in Col-0 (in blue) plants. The y and x axes display $\log_{10}$ values from adjusted *P* values and $\log_2$ fold changes, respectively. The horizontal dashed line represents the threshold of −Log *P* of 1.3 and the vertical, the $\log_2$ fold change of 1.5. For this analysis, extracts from Col-0 and *skb1-1* mutant background plants expressing *pAGO1:NTE^{AGO1}-GFPGUS* were normalized by total content of protein and NTE^{AGO1}-GFPGUS was immunoprecipitated with anti-GFP magnetic agarose beads. Three biological replicates of each genotype were included in the analysis. (**C**) Bar graph showing enrichment in specific protein clusters after analysing interactors co-immunoprecipitated with NTE^{AGO1}-GFPGUS in *skb1-1* mutant background plants compared with NTE^{AGO1}-GFPGUS in Col-0. A log2 fold change of 6 was chosen for ON/OFF proteins (i.e. not present in co-IPs using Col-0 extracts).

NTE in plants. Collectively, these findings suggest that NTEs in AGOs may serve as a versatile platform regulating protein functionality through sophisticated mechanisms.

The NTE^{AGO1} is a crucial hub for PRMT5 interaction and post-translational modifications

Our comprehensive investigation of *A. thaliana* AGO1 focused on its NTE which works as a regulation node for PTMs. We found that NTE hosts several potential arginine methylation sites, which exhibit significant conservation across the plant kingdom suggesting an evolutionary significance in the function of AGO1. Through the utilization of transgenic lines expressing different NTE^{AGO1} segments and a series of MS experiments, our experimental evidence highlighted that AGO1 undergoes symmetric arginine dimethylation on a defined (R48 to R85) NTE^{AGO1} region.

We showed AGO1 symmetric arginine dimethylation was abolished in *prmt5* mutant plants, thereby verifying PRMT5 as the main responsible for the symmetric arginine dimethylation of AGO1. Furthermore, our investigations unveiled a direct interaction between both proteins. We demonstrated that NTE^{AGO1} was sufficient for this interaction, and its absence resulted in the complete loss of AGO1's ability to interact with PRMT5. Additionally, deletion of the segment (Q111-A196), devoid of any methylation sites, led to a significant reduction in the symmetric dimethylarginine signal, indicating its crucial role during AGO1 methylation. These findings underscore the dual function of the NTE^{AGO1}, not only carrying the targeted arginine residues for methylation but also prompting the interaction with PRMT5.

sDMA and aDMA competition guided by different PRMTs on NTE^{AGO1}

Our experimental studies highlight that R48 and R83 (and possibly R59) were exclusively methylated in a PRMT5-dependent manner. The selective symmetric dimethylation of these three arginine residues suggests a strong specificity of PRMT5 for these sites. At the same time, MS experiments in *skb1-1* mutant plants revealed a positive dimethylated status on R30, R34, R62, R85, R94 and R101. As PRMT5 is the only methyltransferase responsible for sDMA in Arabidopsis, these results indicate that AGO1 also undergoes asymmetric arginine dimethylation triggered by other PRMT proteins.

Seven types of PRMTs have been described for catalyzing asymmetric arginine dimethylation in Arabidopsis (24). It has been shown in animals' cells that the loss of PRMT1 activity leads to an increase in global MMA and sDMA levels. These findings reveal the dynamic interplay between different arginine methylation types in the cells and the pre-existence of the dominant aDMA mark can block sDMA and MMA marks on the same substrate (55). Interestingly, we found that two of the three exclusive sDMA, R59 and R83, are located immediately upstream of a putative aDMA (found in *skb1-1*). This hitherto undescribed binary couple methylation site is so far unique among all eukaryotic AGO superfamily. MS experiments conducted in *skb1-1* mutant plants revealed that in the absence of PRMT5, NTE^{AGO1} could interact with PRMT1A, PRMT1B and PRMT10. These interactions in *skb1-1* mutant plants raise the question of potential competition between both types of PRMTs for NTE^{AGO1} recognition. Since MS analyses performed are not able to differentiate between aDMA and sDMA, we cannot ascertain whether R30, R34, R62, R85, R94 and R101 are exclusively asymmetrically dimethylated when PRMT5 is absent or if it also occurs in wild-type plants. Further investigations should be undertaken to identify the responsible(s) for aDMA marks in AGO1, as well as the hierarchy between both types of PRMTs for substrate recognition.

Lack of PRMT5 drastically reshapes NTE^{AGO1} interactome

The current model proposes AGO1 as a nucleo-cytosolic shuttling protein between a cytoplasmic steady-state and a transient nuclear subcellular localization (14). In light of recent

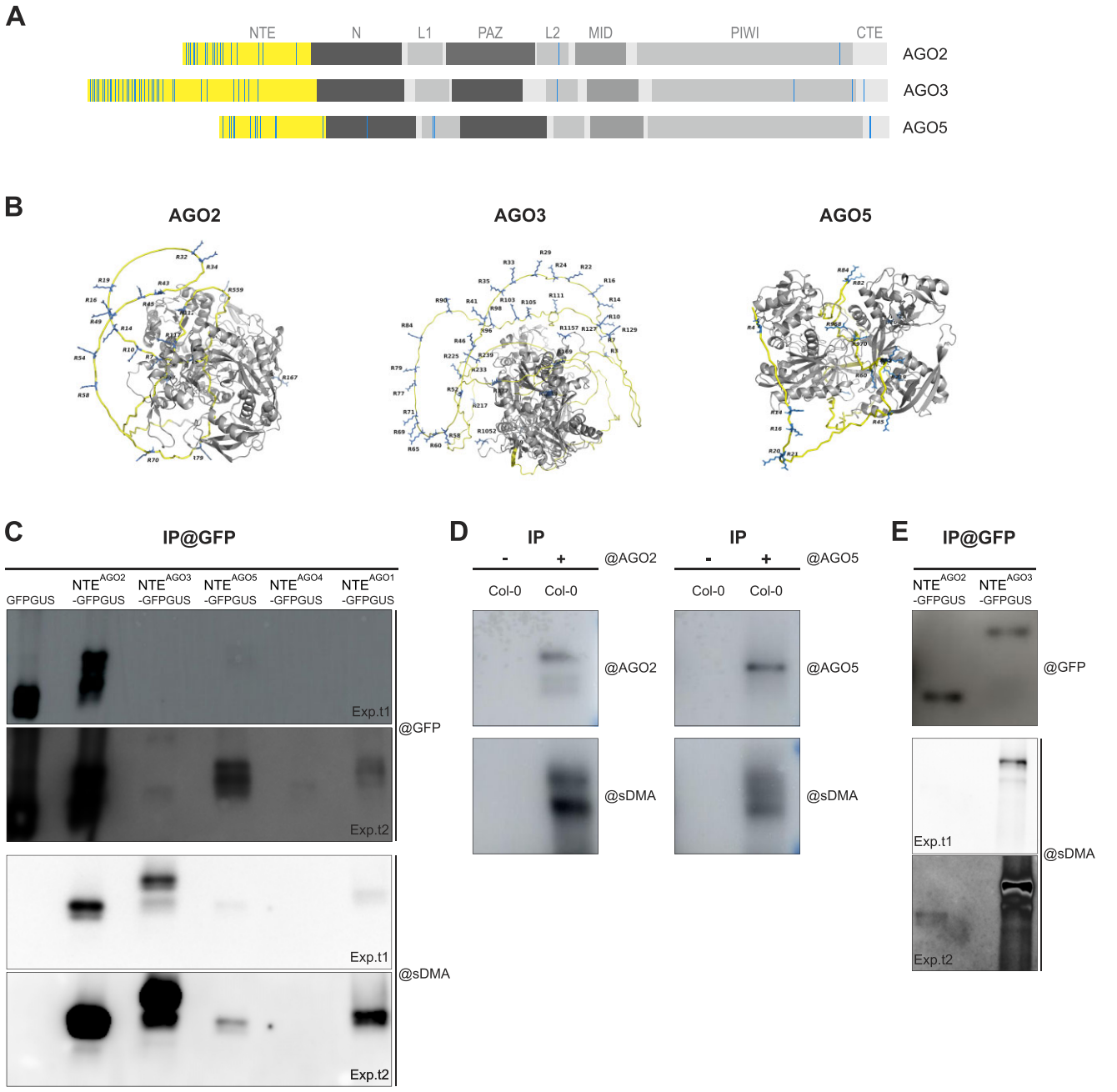

Figure 6. sDMA as a common post-translational modification in Arabidopsis AGO proteins. (**A**) Schematic representation of putative arginine methylation sites predicted for AGO2, AGO3 and AGO5. Globular domains are shown in grey, NTE^{AGOs} in yellow, and putative methylated arginine residues in blue. (**B**) Modelling views of AGO2, AGO3 and AGO5 structures predicted using AlphaFold2. Globular domains are shown in grey cartoon, NTE^{AGOs} in yellow cartoon and ribbon, and the putative methylated arginine residues in blue sticks. (**C**) Western blot assays showing methylation status of transgenic NTEs versions of the different AGOs. Leaves from *N. benthamiana* were processed three days after infiltration, and upon normalization by total content of protein, the different NTEs were immunoprecipitated with anti-GFP magnetic agarose beads. IP fractions were incubated with anti-GFP and anti-sDMA antibody to check transgenic protein expression and methylation status, respectively. Membrane was developed at short (Exp.t1) and long (Exp.t2) exposure times. All NTEs were fused to GFPGUS and expressed under the Cauliflower mosaic virus *35S* promoter in *N. benthamiana*. Expression of GFPGUS and NTE^{AGO4}-GFPGUS were used as negative controls. (**D, E**) Western blot assays showing methylation status of endogenous AGO2 and AGO5 in wild-type background (Col-0), or transgenic NTE^{AGO2} and NTE^{AGO3} in Arabidopsis plants. Upon normalization of plant extracts by total content of protein, endogenous AGO2 and AGO5 were immunoprecipitated with the specified anti-AGO antibody (D), while transgenic versions, with anti-GFP magnetic agarose beads (E). IP fractions were incubated with the corresponding antibody, and with anti-sDMA antibody to test methylation status. Transgenic versions of NTE^{AGO2} and NTE^{AGO3} fused to GFPGUS were cloned under their respective endogenous promoter. Membrane was developed at short (Exp.t1) and long (Exp.t2) exposure times.

descriptions indicating that sDMA and aDMA can elicit opposing biological effects (50), we opted to explore AGO1 behaviour in the absence of PRMT5, which exclusively eliminates sDMA. Our findings indicate that the nuclear shuttling of AGO1 remains unaffected in the *skb1-1* mutant plants. Additionally, we determined that the abolition of the AGO1 nuclear export process did not impede the PRMT5-AGO1 interaction, confirming that this interaction may occur in both the nucleus and cytoplasm. Regarding AGO1's loading, we provided evidence that the global loading of miRNAs into AGO1 remained largely unchanged in the absence of sDMA. However, our studies cannot exclude the possibility that in the absence of sDMA, aDMA may still serve redundant functions in regulating AGO1 subcellular localization or miRNA loading. Intriguingly, a subset of siRNAs, primarily 22nt-long derived from protein-coding genes, were prevented from loading into AGO1 in *prmt5* mutant plants.

Furthermore, our studies also reveal that the absence of PRMT5 drastically reshapes the NTE^{AGO1} interactome. This shift in the interactome could explain the depletion of specific siRNAs, affecting the interaction of AGO1 with proteins involved in siRNA loading. IP-MS studies identified a global enrichment of protein interactions in NTE^{AGO1}/*skb1-1*. Remarkably, many belong to major clusters already associated with AGO pathways, such as protein translation, mRNA splicing, the RNA Pol II complex, and protein stability/turnover, among others. While further studies need to be performed to understand the specific role of AGO1 symmetric arginine dimethylation during these processes, the enrichment in the interaction of the NTE^{AGO1} with deubiquitylation and proteasome-related proteins suggests the arginine methylations could play a role in maintaining the normal cellular homeostatic equilibrium of AGO1. It has been described that AGO1 ubiquitylation promotes its degradation by the autophagy pathway (18). Therefore, similar to the recent findings for *At*-AGO2, the absence of symmetric arginine dimethylation could promote deubiquitylation and stabilize AGO1 (54). Given that AGO1 possesses a complex self-regulation network to control protein levels in both non-stress and stress situations, it is possible that this highly-regulated mechanism masks the direct effect of sDMA on AGO1 stability.

Arginine methylation patterns suggest a common regulatory mechanism in plant AGO proteins

Sequence alignments of AGO proteins revealed notable variability in the length and amino acid composition of NTE^{AGOs} compared to the remaining domains. Previous studies have identified different roles of the NTE^{AGOs} in Arabidopsis; however, they have always been restricted to individual AGO proteins. Our study confirmed that NTE of AGO1, AGO2, AGO3 and AGO5, undergo symmetric arginine dimethylation. Furthermore, we showed that these methylation sites were conserved among AGO orthologs in several plant species, indicating possible regulatory similarities.

Remarkably, none of the AGO proteins mainly involved in nuclear TGS (AGO4, 6, 8 and 9; Clade III) were identified as potential candidates for arginine methylation. On the contrary, AGO1 and AGO5 (Clade I), and AGO2 and AGO3 (Clade II), all mainly involved in PTGS showed sDMA modifications. Beyond the very low sequence conservation along NTEs, our studies have shown AGO1/AGO5 and AGO2/AGO3 share a similar pattern of putative methylation sites between clade members. Also, they show strong conservation among different orthologs from several plant species. These results suggest that arginine methylation could serve as a common regulatory checkpoint, which could influence protein interaction, stability, and turnover of PTGS-related AGOs. Furthermore, the possibility of shared regulatory mechanisms through arginine methylation prompts research into the potential interplay between different types of arginine modifications, PRMT proteins, interacting partners, and other PTMs extending the understanding of AGOs functions and regulatory networks in plant gene silencing pathways.

Data availability

Sequencing data have been deposited into BioProject/SRA. Accession to cite for these SRA data: PRJNA1034069. qPCR data in Zenodo repository under doi:10.5281/zenodo.10912535 The models of AGO proteins are available in ModelArchive with the accession codes ma-9tjqm, ma-5qyie, ma-plafl, ma-b22as and ma-r2taa. The mass spectrometry proteomics data have been deposited to the ProteomeXchange Consortium via the PRIDE partner repository with the dataset identifier PXD049971.

Supplementary data

Supplementary Data are available at NAR Online.

Acknowledgements

We thank R. Rocamora, V. Sanchez and R. Lozano-Durán for providing plasmids; J. Azevedo-Favory, E. Gutiérrez-Beltrán and J. Questa for sharing antibodies, J.A. Navarro, and I. Andreu for fruitful discussion; the CRG/UPF Proteomics Unit, R. Ursache, F. Fenselau de Felippes and the Bologna group for critical reading and discussions.

Author contributions: A.M.-M., A.L. and N.G.B. conceived the experiments. A.M.-M. and A.L. performed the experiments. C.E. performed sequence analyses, molecular modelling, and protein simulations. B.M. contributed biological material. V.M.G.-M. performed RNA sequencing, computational and statistical analyses. G.L.R. performed proteomics data analysis. A.M.-M., A.L. and N.G.B. wrote the manuscript.

Funding

A.M.-M. is recipient of predoctoral grant [PRE2019-087615] funded by MCIN/AEI /10.13039/501100011033 and by "ESF Investing in your future. C.E. receives the predoctoral fellowship HORIZON-MSCA-2021-COFUND-01 rePLANT-GA101081581 Funded by the European Union. Views and opinions expressed are however those of the author(s) only and do not necessarily reflect those of the European Union or the EUROPEAN RESEARCH EXECUTIVE AGENCY (REA). Neither the European Union nor the granting authority can be held responsible for them. B.M. has received funding by the following postdoctoral fellowships: the "Severo Ochoa Programme" [SEV-2015-0533 funded by MICIU/AEI /10.13039/501100011033, the fellowship [FJC2018-036091-I], funded by MICIU/AEI /10.13039/501100011033, the programme "Beatriu de Pinós

[2019 BP 00159], funded by the Secretary of Universities and Research (Government of Catalonia), and by the Horizon 2020 programme of research innovation of the European Union under the Marie Sklodowska-Curie grant agreement [Nº 801370]. Also this project has received funding from the European Union's Horizon 2020 research and innovation programme under the Marie Sklodowska-Curie grant agreement No 896320 – AGOras through the Postdoctoral Fellowship awarded to B.M. by the H2020-MSCA-IF-2019 programme. N.G.B. was supported by Grant [RYC2020-029185-], funded by MCIN/AEI /10.13039/501100011033 and by "ESF Investing in your future". The project that gave rise to these results received the support of afellowship from "la Caixa" Foundation (ID100010434). The fellowship code awarded to N.G.B. is: LCF/BQ/PI19/11690007. The project that gave rise to these results received the support of Grant [PGC2018-101075-A-I00], funded by MICIU/AEI/10.13039/ 501100011033 and by "ERDF A way of making Europe, Grant [EUR2020-112097], funded by MICIU/AEI/10.13039/501100011033 and by "European Union NextGenerationEU/PRTR, the SGR program [2021 SGR 01066], funded by Direcció General de Recerca (DGR) del Departament de Recerca i Universitats (REU)" and by the CERCA Programme/Generalitat de Catalunya. The N.G.B. laboratory also acknowledges the support from the CERCA Programme/Generalitat de Catalunya and from Ministerio De Ciencia e Innovación/Agencia Estatal de Investigación. (AEI), through the "Severo Ochoa Programme for Centres of Excellence in R&D" [SEV-2015-0533] and [CEX2019-000902-S] funded by MICIU/AEI /10.13039/501100011033.

Conflict of interest statement

None declared.

References

1. Bologna,N.G. and Voinnet,O. (2014) The diversity, biogenesis, and activities of endogenous silencing small RNAs in Arabidopsis. *Annu. Rev. Plant Biol.*, **65**, 473–503.
2. Zhan,J. and Meyers,B.C. (2023) Plant small RNAs: their biogenesis, regulatory roles, and functions. *Annu. Rev. Plant Biol.*, **74**, 21–51.
3. Fang,X. and Qi,Y. (2016) RNAi in plants: an argonaute-centered view. *Plant Cell*, **28**, 272–285.
4. Zhang,H., Xia,R., Meyers,B.C. and Walbot,V. (2015) Evolution, functions, and mysteries of plant ARGONAUTE proteins. *Curr. Opin. Plant Biol.*, **27**, 84–90.
5. Nakanishi,K. (2022) Anatomy of four human Argonaute proteins. *Nucleic Acids Res.*, **50**, 6618–6638.
6. Poulsen,C., Vaucheret,H. and Brodersen,P. (2013) Lessons on RNA Silencing Mechanisms in Plants from Eukaryotic Argonaute Structures. *Plant Cell*, **25**, 22–37.
7. Kwak,P.B. and Tomari,Y. (2012) The N domain of Argonaute drives duplex unwinding during RISC assembly. *Nat. Struct. Mol. Biol.*, **19**, 145–151.
8. Frank,F., Hauver,J., Sonenberg,N. and Nagar,B. (2012) Arabidopsis Argonaute MID domains use their nucleotide specificity loop to sort small RNAs. *EMBO J.*, **31**, 3588–3595.
9. Schirle,N.T. and MacRae,I.J. (2012) The crystal structure of human Argonaute2. *Science*, **336**, 1037–1040.
10. Hutvagner,G. and Simard,M.J. (2008) Argonaute proteins: key players in RNA silencing. *Nat. Rev. Mol. Cell Biol.*, **9**, 22–32.
11. Martín-Merchán,A., Moro,B., Bouet,A. and Bologna,N.G. (2023) Domain organization, expression, subcellular localization, and biological roles of ARGONAUTE proteins in Arabidopsis. *J. Exp. Bot.*, **74**, 2374–2388.
12. Vaucheret,H. (2008) Plant ARGONAUTES. *Trends Plant Sci.*, **13**, 350–358.
13. Brodersen,P., Sakvarelidze-Achard,L., Schaller,H., Khafif,M., Schott,G., Bendahmane,A. and Voinnet,O. (2012) Isoprenoid biosynthesis is required for miRNA function and affects membrane association of ARGONAUTE 1 in Arabidopsis. *Proc. Natl. Acad. Sci. U.S.A.*, **109**, 1778–1783.
14. Bologna,N.G., Iselin,R., Abriata,L.A., Sarazin,A., Pumplin,N., Jay,F., Grentzinger,T., Dal Peraro,M. and Voinnet,O. (2018) Nucleo-cytosolic shuttling of ARGONAUTE1 prompts a revised model of the plant MicroRNA pathway. *Mol. Cell*, **69**, 709–719.
15. Xu,Y., Zhang,Y., Li,Z., Soloria,A.K., Potter,S. and Chen,X. (2023) The N-terminal extension of Arabidopsis ARGONAUTE 1 is essential for microRNA activities. *PLoS Genet.*, **19**, e1010450.
16. Bressendorff,S., Kausika,S., Sjøgaard,I., Oksbjerg,E., Michels,A., Poulsen,C. and Brodersen,P. (2023) The N-coil and the globular N-terminal domain of plant ARGONAUTE1 are interaction hubs for regulatory factors. *Biochem. J.*, **480**, 957–974.
17. Vaucheret,H., Mallory,A.C. and Bartel,D.P. (2006) AGO1 homeostasis entails coexpression of MIR168 and AGO1 and preferential stabilization of miR168 by AGO1. *Mol. Cell*, **22**, 129–136.
18. Derrien,B., Baumberger,N., Schepetilnikov,M., Viotti,C., De Cillia,J., Ziegler-Graff,V., Isono,E., Schumacher,K. and Genschik,P. (2012) Degradation of the antiviral component ARGONAUTE1 by the autophagy pathway. *Proc. Natl. Acad. Sci. U.S.A.*, **109**, 15942–15946.
19. Hacquard,T., Clavel,M., Baldrich,P., Lechner,E., Pérez-Salamó,I., Schepetilnikov,M., Derrien,B., Dubois,M., Hammann,P., Kuhn,L., *et al.* (2022) The Arabidopsis F-box protein FBW2 targets AGO1 for degradation to prevent spurious loading of illegitimate small RNA. *Cell Rep.*, **39**, e110671.
20. de la Fuente van Bentem,S., Anrather,D., Dohnal,I., Roitinger,E., Csaszar,E., Joore,J., Buijnink,J., Carreri,A., Forzani,C., Lorkovic,Z.J., *et al.* (2008) Site-Specific Phosphorylation Profiling of Arabidopsis Proteins by Mass Spectrometry and Peptide Chip Analysis. *J. Proteome Res.*, **7**, 2458–2470.
21. Bedford,M.T. and Clarke,S.G. (2009) Protein arginine methylation in mammals: who, what, and why. *Mol. Cell*, **33**, 1–13.
22. Fulton,M.D., Brown,T. and Zheng,Y.G. (2019) The biological axis of protein arginine methylation and asymmetric dimethylarginine. *Int. J. Mol. Sci.*, **20**, 3322.
23. Gayatri,S. and Bedford,M.T. (2014) Readers of histone methylarginine marks. *Biochim. Biophys. Acta*, **1839**, 702–710.
24. Ahmad,A. and Cao,X. (2012) Plant PRMTs broaden the scope of arginine methylation. *J. Genet. Genomics*, **39**, 195–208.
25. Blanc,R.S. and Richard,S. (2017) Arginine methylation: the coming of age. *Mol. Cell*, **65**, 8–24.
26. Tripsianes,K., Madl,T., Machyna,M., Fessas,D., Englbrecht,C., Fischer,U., Neugebauer,K. and Sattler,M. (2011) Structural basis for dimethylarginine recognition by the Tudor domains of human SMN and SPF30 proteins. *Nat. Struct. Mol. Biol.*, **18**, 1414–1420.
27. dit Frey,N.F., Muller,P., Jammes,F., Kizis,D., Leung,J., Perrot-Rechenmann,C. and Bianchi,M.W. (2010) The RNA binding protein Tudor-SN is essential for stress tolerance and stabilizes levels of stress-responsive mRNAs encoding secreted proteins in Arabidopsis. *Plant Cell*, **22**, 1575–1591.
28. Vagin,V.V., Hannon,G.J. and Aravin,A.A. (2009) Arginine methylation as a molecular signature of the Piwi small RNA pathway. *Cell Cycle*, **8**, 4003–4004.
29. Kirino,Y., Kim,N., de Planell-Saguer,M., Khandros,E., Chiorean,S., Klein,P.S., Rigoutsos,I., Jongens,T.A. and Mourelatos,Z. (2009) Arginine methylation of Piwi proteins catalysed by dPRMT5 is required for Ago3 and Aub stability. *Nat. Cell Biol.*, **11**, 652–658.

30. Zhang,H., Liu,K., Izumi,N., Huang,H., Ding,D., Ni,Z., Sidhu,S.S., Chen,C., Tomari,Y. and Min,J. (2017) Structural basis for arginine methylation-independent recognition of PIWIL1 by TDRD2. *Proc. Natl. Acad. Sci. U.S.A.*, **114**, 12483–12488.
31. Nguyen,D.A.H. and Phillips,C.M. (2021) Arginine methylation promotes siRNA-binding specificity for a spermatogenesis-specific isoform of the Argonaute protein CSR-1. *Nat. Commun.*, **12**, 4212.
32. Hu,P., Zhao,H., Zhu,P., Xiao,Y., Miao,W., Wang,Y. and Jin,H. (2019) Dual regulation of Arabidopsis AGO2 by arginine methylation. *Nat. Commun.*, **10**, 844.
33. Katzen,F. (2007) Gateway® recombinational cloning: a biological operating system. *Expert Opin. Drug Discov.*, **2**, 571–589.
34. Clough,S.J. and Bent,A.F. (1998) Floral dip: a simplified method for Agrobacterium-mediated transformation of Arabidopsis thaliana. *Plant J.*, **16**, 735–743.
35. Schindelin,J., Arganda-Carreras,I., Frise,E., Kaynig,V., Longair,M., Pietzsch,T., Preibisch,S., Rueden,C., Saalfeld,S., Schmid,B., *et al.* (2012) Fiji: an open-source platform for biological-image analysis. *Nat. Methods*, **9**, 676–682.
36. Chiva,C., Olivella,R., Borras,E., Espadas,G., Pastor,O., Sole,A. and Sabido,E. (2018) QCloud: a cloud-based quality control system for mass spectrometry-based proteomics laboratories. *PLoS One*, **13**, e0189209.
37. Perkins,D.N., Pappin,D.J.C., Creasy,D.M. and Cottrell,J.S. (1999) Probability-based protein identification by searching sequence databases using mass spectrometry data. *Electrophoresis*, **20**, 3551–3567.
38. Beer,L.A., Liu,P., Ky,B., Barnhart,K.T. and Speicher,D.W. (2017) Efficient quantitative comparisons of plasma proteomes using label-free analysis with MaxQuant. *Methods Mol. Biol.*, **1619**, 339–352.
39. Kuhn,L., Vincent,T., Hammann,P. and Zuber,H. (2023) Exploring Protein Interactome Data with IPinquiry: statistical Analysis and Data Visualization by Spectral Counts. *Methods Mol. Biol.*, **2426**, 243–265.
40. Shannon,P., Markiel,A., Ozier,O., Baliga,N.S., Wang,J.T., Ramage,D., Amin,N., Schwikowski,B. and Ideker,T. (2003) Cytoscape: a software environment for integrated models of biomolecular interaction networks. *Genome Res.*, **13**, 2498–2504.
41. Perez-Riverol,Y., Bai,J., Bandla,C., García-Seisdedos,D., Hewapathirana,S., Kamatchinathan,S., Kundu,D.J., Prakash,A., Frericks-Zipper,A., Eisenacher,M., *et al.* (2022) The PRIDE database resources in 2022: a hub for mass spectrometry-based proteomics evidences. *Nucleic Acids Res.*, **50**, D543–D552.
42. Zheng,W., Wuyun,Q., Cheng,M., Hu,G. and Zhang,Y. (2020) Two-level protein methylation prediction using structure model-based features. *Sci. Rep.*, **10**, 6008.
43. Mirdita,M., Schütze,K., Moriwaki,Y., Heo,L., Ovchinnikov,S. and Steinegger,M. (2022) ColabFold: making protein folding accessible to all. *Nat. Methods*, **19**, 679–682.
44. Robert,X. and Gouet,P. (2014) Deciphering key features in protein structures with the new ENDscript server. *Nucleic Acids Res.*, **42**, W320–W324.
45. Tamura,K., Stecher,G. and Kumar,S. (2021) MEGA11: molecular evolutionary genetics analysis version 11. *Mol. Biol. Evol.*, **38**, 3022–3027.
46. Edgar,R.C. (2004) MUSCLE: multiple sequence alignment with high accuracy and high throughput. *Nucleic Acids Res.*, **32**, 1792–1797.
47. Deng,X., Gu,L., Liu,C., Lu,T., Lu,F., Lu,Z., Cui,P., Pei,Y., Wang,B., Hu,S., *et al.* (2010) Arginine methylation mediated by the Arabidopsis homolog of PRMT5 is essential for proper pre-mRNA splicing. *Proc. Natl. Acad. Sci. U.S.A.*, **107**, 19114–19119.
48. Wang,X., Zhang,Y., Ma,Q., Zhang,Z., Xue,Y., Bao,S. and Chong,K. (2007) SKB1-mediated symmetric dimethylation of histone H4R3 controls flowering time in Arabidopsis. *EMBO J.*, **26**, 1934–1941.
49. Wang,H., Straubinger,R.M., Aletta,J.M., Cao,J., Duan,X., Yu,H. and Qu,J. (2009) Accurate localization and relative quantification of arginine methylation using nanoflow liquid chromatography coupled to electron transfer dissociation and drbitrap mass spectrometry. *J. Am. Soc. Mass Spectrom.*, **20**, 507–519.
50. Li,M., An,W., Xu,L., Lin,Y., Su,L. and Liu,X. (2019) The arginine methyltransferase PRMT5 and PRMT1 distinctly regulate the degradation of anti-apoptotic protein CFLARL in human lung cancer cells. *J. Exp. Clin. Cancer Res.*, **38**, 64.
51. Mi,S., Cai,T., Hu,Y., Chen,Y., Hodges,E., Ni,F., Wu,L., Li,S., Zhou,H., Long,C., *et al.* (2008) Sorting of small RNAs into Arabidopsis argonaute complexes is directed by the 5' terminal nucleotide. *Cell*, **133**, 116–127.
52. Vaucheret,H. and Voinnet,O. (2023) The plant siRNA landscape. *Plant Cell*, **36**, 246-275.
53. Gutierrez-Beltran,E., Elander,P.H., Dalman,K., Dayhoff,G.W., Moschou,P.N., Uversky,V.N., Crespo,J.L. and Bozhkov,P.V. (2021) Tudor staphylococcal nuclease is a docking platform for stress granule components and is essential for SnRK1 activation in Arabidopsis. *EMBO J.*, **40**, e105043.
54. Hu,P., Zhao,H., Zhu,P., Xiao,Y., Miao,W., Wang,Y. and Jin,H. (2019) Dual regulation of Arabidopsis AGO2 by arginine methylation. *Nat. Commun.*, **10**, 844.
55. Dhar,S., Vemulapalli,V., Patananan,A.N., Huang,G.L., Di Lorenzo,A., Richard,S., Comb,M.J., Guo,A., Clarke,S.G. and Bedford,M.T. (2013) Loss of the major Type I arginine methyltransferase PRMT1 causes substrate scavenging by other PRMTs. *Sci. Rep.*, **3**, 1311.

Received: November 2, 2023. **Revised:** April 10, 2024. **Editorial Decision:** April 25, 2024. **Accepted:** April 30, 2024